Peyer's patch phagocytes acquire specific transcriptional programs that influence their maturation and activation profiles

Cynthia Arroyo Portilla, Romain Fenouil, Camille Wagner, Cécilia Luciani, Margaux Lagier, Clément da Silva, Fanny Hidalgo-Villeda, Lionel Spinelli, Mathieu Fallet, Julie Tomas, et al.

ARTICLE

Peyer's patch phagocytes acquire specific transcriptional programs that influence their maturation and activation profiles

Cynthia Arroyo Portilla [1,2], Romain Fenouil [1], Camille Wagner [1], Cécilia Luciani [1], Margaux Lagier [1], Clément Da Silva [1], Fanny Hidalgo-Villeda [1,3], Lionel Spinelli [1], Mathieu Fallet [1], Julie Tomas [1], Jean-Pierre Gorvel [1] and Hugues Lelouard [1,✉]

Peyer's patches (PPs) are secondary lymphoid organs in contact with the external environment via the intestinal lumen, thus combining antigen sampling and immune response initiation sites. Therefore, they provide a unique opportunity to study the entire process of phagocyte differentiation and activation *in vivo*. Here, we deciphered the transcriptional and spatial landscape of PP phagocyte populations from their emergence in the tissue to their final maturation state at homeostasis and under stimulation. Activation of monocyte-derived Lysozyme-expressing dendritic cells (LysoDCs) differs from that of macrophages by their upregulation of conventional DC (cDC) signature genes such as *Ccr7* and downregulation of typical monocyte-derived cell genes such as *Cx3cr1*. We identified gene sets that distinguish PP cDCs from the villus ones and from LysoDCs. We also identified key immature, early, intermediate, and late maturation markers of PP phagocytes. Finally, exploiting the ability of the PP interfollicular region to host both villous and subepithelial dome emigrated cDCs, we showed that the type of stimulus, the subset, but also the initial location of cDCs shape their activation profile and thus direct the immune response. Our study highlights the importance of targeting the right phagocyte subset at the right place and time to manipulate the immune response.

Mucosal Immunology (2023) 16:527–547; https://doi.org/10.1016/j.mucimm.2023.05.009

INTRODUCTION

Peyer's patches (PPs) are the major immunoinductive sites of the mammalian small intestine[1]. Comprising multiple B cell follicles forming domes at the surface of the mucosa interspersed with dome-associated villi (DAVs) above interfollicular regions (IFRs) enriched in naïve T cells, PPs excel in the generation of the antigen-specific immunoglobulin (Ig)A-secreting cells that populate the villus lamina propria[2,3]. PPs must distinguish pathogens from the vast majority of innocuous antigens derived from food and microbiota. Detection of pathogens and initiation of an appropriate immune response relies on a complex network of mononuclear phagocytes[4]. As PPs combine antigen uptake and immune inductive sites, they offer a unique opportunity among secondary lymphoid organs to follow the entire process of phagocyte differentiation and activation in a single tissue, including their antigen sampling, migration, and B and T-cell priming. Three main families of phagocytes have been documented in PPs: plasmacytoid dendritic cells (pDCs), conventional DCs (cDCs), and monocyte-derived phagocytes. Each of these families has specific characteristics that are unique to PPs. For example, monocyte-derived cells of human and mouse PPs include DCs called lysozyme-expressing DCs or LysoDCs, which so far have no equivalent in other tissues[5–7]. LysoDCs are mainly located in the subepithelial dome (SED), whereas PP macrophages termed LysoMacs are present in both SED and IFR[6]. LysoDCs and LysoMacs share many functional characteristics, such as high phagocytic activities and strong innate defense mechanisms[6]. They represent the first line of defense below the follicle-associated epithelium (FAE), which contains the specialized epithelial cells called M cells that are responsible for transporting antigens from the lumen to the SED. LysoDCs cooperate with M cells to sample antigens by extending dendrites through M cell-specific transcellular pores[8]. Unlike LysoMacs, mature LysoDCs are capable of priming naïve helper T cells[6]. However, only activated LysoDCs express the chemokine receptor CCR7 and migrate to the IFRs where naïve T cells reside, suggesting that the T-cell priming activity of LysoDCs *in vivo* is tightly regulated and dependent on the sensing of a stimulatory signal[7]. In addition to helper T-cell priming toward interferon (IFN)γ and interleukin (IL)-17 production[6,9], LysoDCs can cross-present antigens to induce a cytotoxic T-cell response when stimulated by the complement fragment C5a[10].

Among cDCs, type 1 cDCs (cDC1s) expressing CD8a, XCR1, and CLEC9A are mainly located in the IFRs[11,12], whereas type 2

[1]Aix Marseille Univ, CNRS, INSERM, Centre d'Immunologie de Marseille-Luminy (CIML), Marseille, France. [2]Departamento de Análisis Clínicos, Facultad de Microbiología, Universidad de Costa Rica, San José, Costa Rica. [3]Escuela de Microbiología, Facultad de Ciencias, Universidad Nacional Autónoma de Honduras, Tegucigalpa, Honduras. ✉email: lelouard@ciml.univ-mrs.fr

Received: 26 April 2023 Accepted 23 May 2023
Published online: 29 May 2023

cDCs (cDC2s) expressing SIRPα are located both in the IFRs and in the lower parts of the SED[4,13]. cDC2s form a very heterogeneous population, probably due to their differentiation state and dual location. Thus, immature cDC2s lack CD11b expression but express CCR6, which favors their location in the SED, whereas mature cDC2s express CD11b, increase the surface expression of major histocompatibility complex of class II (MHCII), but also of CCR7, to migrate to the IFRs[13]. In DAVs, cDCs and macrophages are similar to those in classical villi[4]. However, unlike classical villus cDC2s, DAV cDC2s do not migrate to the mesenteric lymph nodes (MLNs) upon stimulation, but to the IFRs, as do SED cDC2s[7,13]. For simplicity, all phagocytes located in the SED, follicle, and IFR will be referred to as dome phagocytes as opposed to DAV phagocytes.

Activation kinetics of cDCs *in vivo* differs from those of LysoDCs, suggesting that the immune response in PP is initiated by a well-orchestrated sequence of events that occur in specific time windows[7]. However, so far only toll-like receptor (TLR7) stimulation of PP has been performed and the process of activation of all PP phagocyte populations under different conditions of stimulation and how this might lead to different responses has not been addressed. Here, we investigated the spatiotemporal landscape of PP phagocytes at homeostasis and upon stimulation *in vivo* with the ligands of TLR7 and TLR9. We defined markers for each phagocyte subset at different stages of differentiation and activation. Finally, we showed that activated DAV cDCs differ from activated dome cDCs, although they migrate to the same site, suggesting that their activation profile is definitively imprinted by their initial site of residence.

RESULTS

Steady-state scRNAseq analysis of PP CD11c^{hi} phagocytes reveals the minimal gene signature that distinguishes mouse monocyte-derived DCs from cDCs

Although the transcriptional profile of LysoDCs has been established at the single-cell level[7], a high-resolution view of the whole PP CD11c^{hi}MHCII^{+} phagocyte system is still lacking. We sought to isolate PP CD11c^{hi}MHCII^{+} phagocytes and analyze their transcriptional profiles by single-cell RNA sequencing (scRNAseq). Since SIRPα^{+} cDC2s represent about 60% of PP phagocytes[13], we decided to discard half of them (Supplementary Fig. 1A and Supplementary Table 1) to allow a better representation of the other subsets (cDC1s, LysoDCs, and LysoMacs).

Uniform manifold approximation and projection (UMAP) embedding of the data identified a small isolated cluster and three groups of multiple clusters (Fig. 1A). The first group consisted of monocyte-derived cells and specifically expressed *Mafb*, *Cx3cr1*, *Mertk,* and *Msr1* (Fig. 1B). In agreement with previous reports[7,13], monocyte-derived cells represented 28% of the total PP phagocytes. They expressed fewer ribosomal genes but paradoxically more genes and transcripts (UMI) than the other groups (Fig. 1A). As expected from their lack of Fcγ receptor I/CD64 expression[14], *Fcgr1* was not detected in PP monocyte-derived cells but another Fcγ receptor gene *Fcgr3* was highly expressed by all monocyte-derived cells (Supplementary Fig. 1B). PP monocyte-derived cells are also known for their strong expression of lysozyme and Bst2[6], which genes (*Lyz1*, *Lyz2* and *Bst2*) were indeed enriched in this group although expressed by the other phagocytes (Fig. 1B and Supplementary Fig. 1B). Monocyte-derived cells also highly expressed *Csf1r*, which encodes the CSF1 receptor involved in the differentiation and survival of monocyte-derived cells (Fig. 1B). Consistent with their role in phagocytosis of particulate antigens[5–8], monocyte-derived cells specifically expressed the gene involved in the phagocytic cup formation *Gas7*[15] (Supplementary Fig. 1C). They were also strikingly enriched for genes of the lysosomal machinery, such as those encoding the lysosomal-associated membrane proteins LAMP1 and LAMP2 and the lysosomal proteases involved in antigen degradation, cathepsin A, B, C, D, F, L, S and X (Supplementary Fig. 1C and not shown). Finally, the gene encoding cystatin F (*Cst7*), a regulator of the activity of cysteine cathepsins, in particular cathepsins L, S, and X, was upregulated in monocyte-derived cells (Supplementary Fig. 1C).

Monocyte-derived cells consisted of two main clusters corresponding to LysoDCs and LysoMacs. As expected, LysoDCs expressed much higher levels of genes encoding proteins of the MHCII presentation pathway (e.g. *H2-Ab1* and *H2-DMb2*) whereas LysoMacs specifically expressed *Cd4* (Fig. 1C). LysoMacs are also known to express some complement machinery genes more strongly than LysoDCs[6]. Indeed, LysoMacs specifically expressed *C2* and *C3* (Fig. 1C and not shown). As previously reported[7], most LysoDCs but no LysoMacs expressed *Emb*, which encodes embigin (Fig. 1C). In addition, LysoDCs were enriched for the expression of *Ccr2* (Fig. 1C), the chemokine receptor required for their recruitment to PP[6]. Finally, LysoDCs were the major producers of *Il22ra2*, which encodes IL-22BP (Fig. 1C), an inhibitor of the IL-22 pathway that promotes antigen uptake in PP[16].

The other two UMAP groups and the small cluster of PP phagocytes consisted of cDCs characterized by the specific expression of *Zbtb46*, *Flt3*, *Btla*, *Kit, Anpep, Kmo* and *Spint2*, although *Btla* and *Kit* were only weakly expressed in the small cluster (Fig. 1D). Many genes of the so-called mouse cDC gene signature[17], such as *Amica1, Ass1, Bri3bp, Cbfa2t3, Cnn2, Pstpip1*, *Traf1* and genes of the MHCII presentation pathway, were enriched in cDCs but were also expressed by LysoDCs, the monocyte-derived phagocytes closest to cDCs in mice (Supplementary Fig. 1D). Other genes in this signature, such as *Adam19*, *Adgrg5*, *Dpp4, Fgl2, Gpr68, H2-Q6, Napsa, Runx3* and *Tbc1d8*, could not even distinguish PP cDCs from monocyte-derived cells (Supplementary Figs. 1D and 1E). We confirmed by flow cytometry that the recently proposed cDC-specific marker CD26[18,19] encoded by *Dpp4* was indeed expressed by both LysoDCs and LysoMacs in addition to cDCs (Supplementary Fig. 1E). Therefore, CD26 should not be considered as a specific cDC marker in PPs. Finally, from the initial cDC signature, only 17 genes showed a strict specificity for cDCs in PPs, of which only *Anpep*, *Flt3*, *Spint2,* and *Zbtb46* showed an almost equal distribution across all cDC clusters (Fig. 1D and Supplementary Fig. 1D).

The minor cDC group (7% of the total PP phagocytes; Fig. 1A) expressed typical cDC1 marker genes, such as *Xcr1*, *Clec9a*, *Cd8a*, *Cadm1*, *Tlr3* and *Clec12a* (Fig. 1E). The transcription factor involved in cDC1 commitment, *Irf8*, was also enriched in this group, although expressed by monocyte-derived cells.

The prominent cDC group and the small isolated cluster, together representing 65% of the total PP phagocytes (Fig. 1A), shared genes with monocyte-derived cells, such as *Sirpa*, suggesting that they were cDC2s (Fig. 1F). As expected from previous studies[6,7,13], they also shared the expression of *Emb*, *Clec4a4* and *F11r* with LysoDCs but not with LysoMacs (Fig. 1C and 1F). However, expression of *Epcam*, a recently described marker of dome cDC2[13], was specific to all but one cDC2 cluster and was not shared with any other PP phagocyte subset (Fig. 1F). Unexpectedly, we also found that the gene

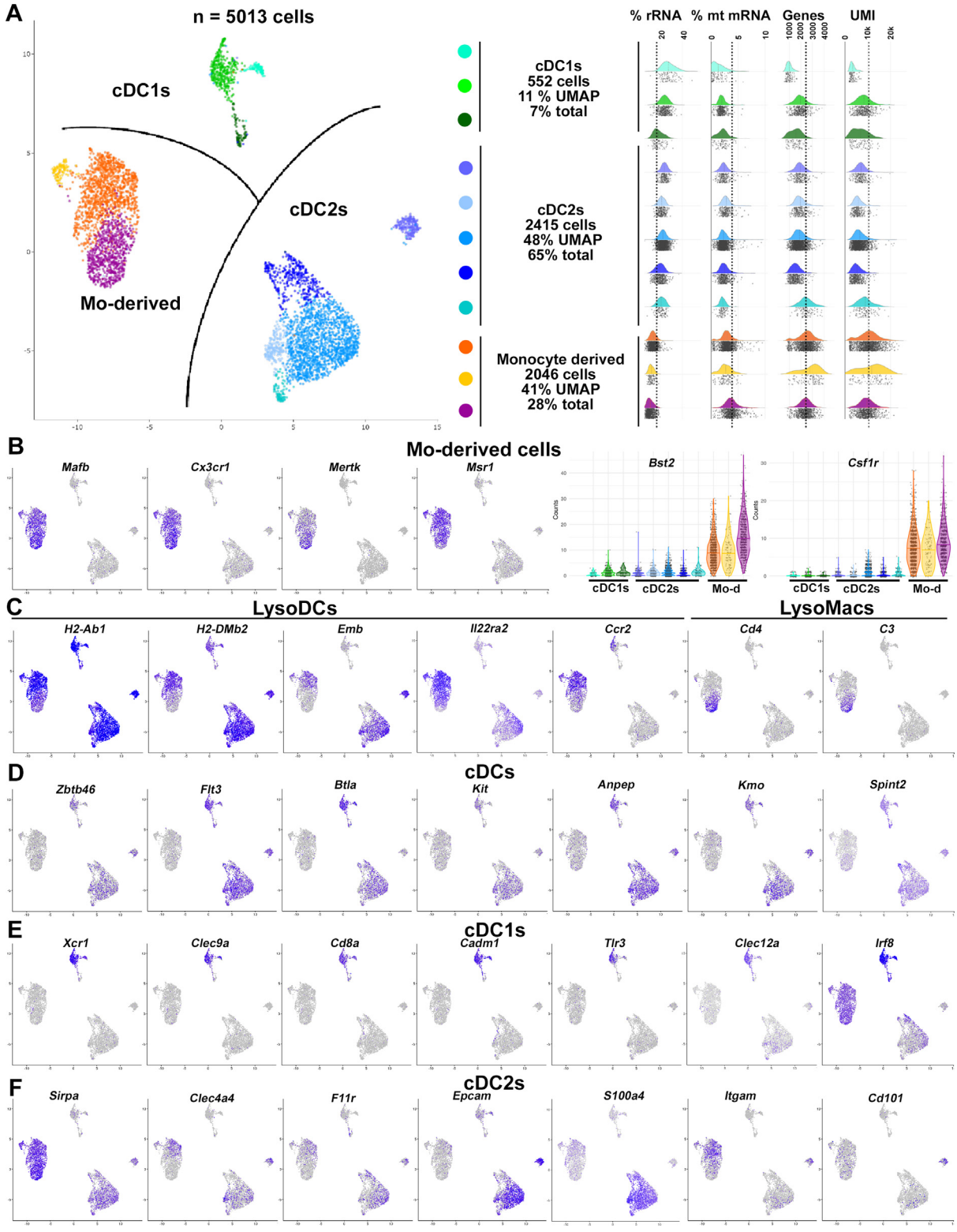

Fig. 1 Steady-state single-cell RNA sequence analysis of Peyer's patch CD11c^{hi} phagocytes. (A–F) Single-cell mRNA sequence analysis of 5013 PP CD11c^{hi} phagocytes extracted from 12 C57Bl/6 mice. (A) UMAP embedding map colored by Seurat clustering shows a small isolated cluster of cDC2s and three groups of multiple clusters representing monocyte-derived cells (Mo-derived; yellow, orange and magenta clusters), cDC1s (shades of green), and cDC2s (shades of blue). The number of cells for each type of phagocytes is indicated in the middle column as well as the ratio it represents in the UMAP and in the total phagocytes, considering that half of the cDC2s were discarded. Histograms on the right show the ratio of r and mt RNA and the number of genes and UMI detected in each cluster. (B–F) Projection of the expression of monocyte-derived cell (B), LysoDC and LysoMac (C), cDC (D), cDC1 (E), and cDC2 (F) marker genes onto the UMAP or cluster violin plots show the transcriptional specificities of each phagocyte subset. See also Supplementary Fig. S1 for gating strategy and additional gene expression in Peyer's patches phagocytes. cDC = conventional dendritic cell; mRNA = messenger RNA; mt = mitochondrial; r = ribosomal; UMAP = uniform manifold approximation and projection; UMI = unique molecular identifier.

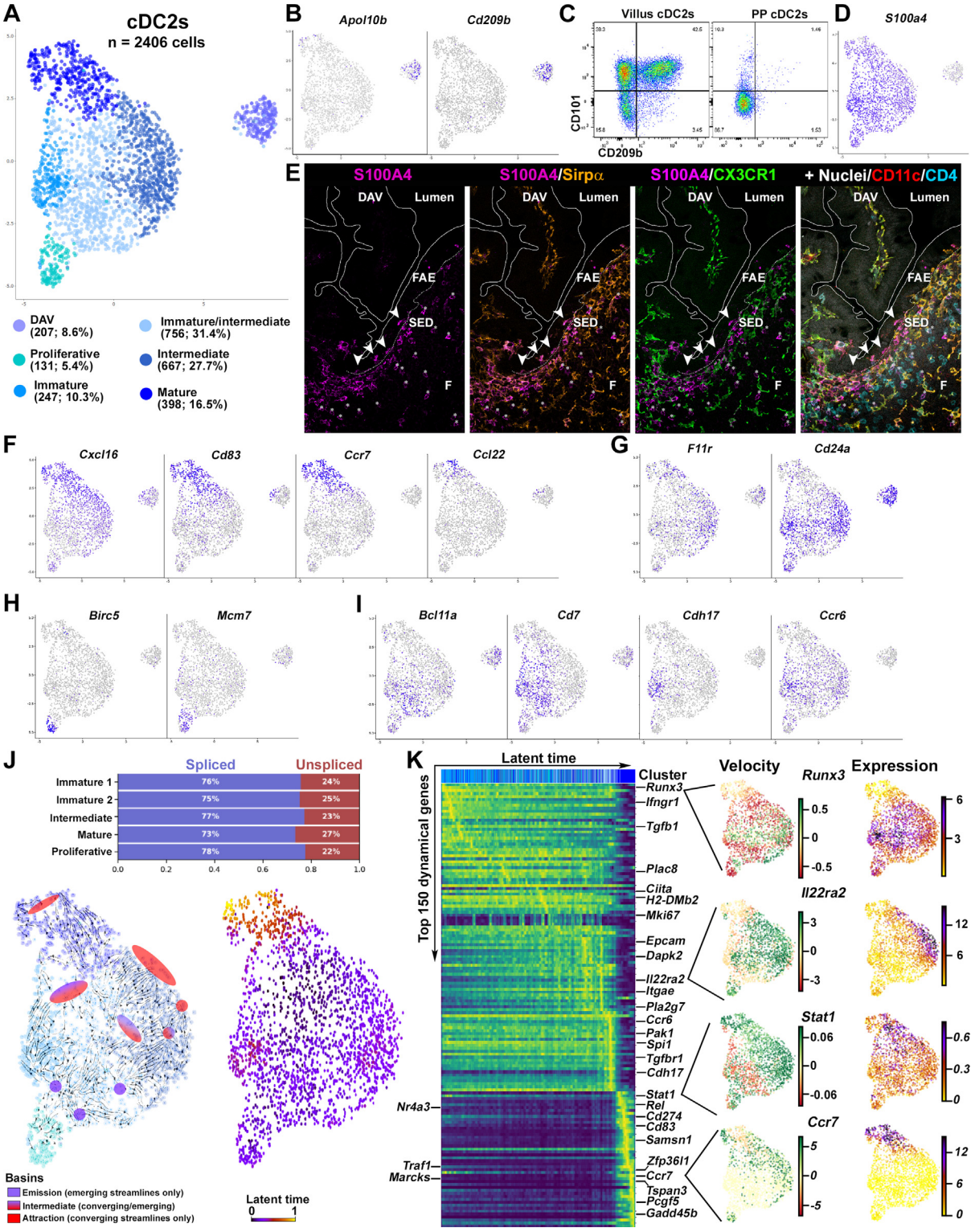

encoding S100A4, a protein involved in M cell maturation and originally thought to be expressed mainly by PP LysoDCs, LysoMacs and type 3 innate lymphoid cells[20], was predominantly expressed by the prominent group of cDC2s (Fig. 1F). Finally, in agreement with previously published data[13], the CD11b gene *Itgam* was expressed at very low levels by few cDC2s of the prominent cDC2 group as compared to LysoDCs, suggesting a very transient expression of this integrin in PP cDC2s (Fig. 1F).

Nevertheless, *Itgam* was expressed at high levels by the small isolated cDC2 cluster. Since CD11b is known to be highly expressed by both LysoDCs and DAV cDC2s compared to dome cDC2s[13], we hypothesized that this cluster consisted of DAV cDC2s, which, unlike dome cDC2s, also express CD101[13]. *Cd101* was indeed specifically expressed in this cluster, confirming that it was composed of DAV cDC2s (Fig. 1F).

The transcriptional profile of dome cDC2s reveals the chronology of their differentiation and maturation *in vivo*

Next, we subclustered each group of phagocytes to investigate their differentiation pathways, as previously done for LysoDCs[7]. Dome cDC2s were subdivided into five clusters whereas DAV cDC2s represented only one isolated cluster (8.6% of cDC2; Fig. 2A). In addition to *Cd101*, the latter was particularly characterized by its expression of *Apol10b*, *Cd209b*, *Cxx1b, Gp2*, *Mgl2*, *Siglecf* and of the transcription factor *Runx1* (Fig. 2B and Supplementary Fig. 2A). We confirmed by flow cytometry the specific expression of CD209b by almost half of small intestinal villus CD101$^+$ cDC2s, but not by dome cDC2s, further supporting the identity of the DAV cDC2 cluster (Fig. 2C). In contrast, all dome cDC2s but not DAV cDC2s expressed *S100a4*, which could be the first specific and reliable marker for dome cDC2s (Fig. 2D). Indeed, we confirmed by microscopy the specific expression of S100A4 by both SED and IFR cDC2s (CD11c$^+$SIRPα$^+$CX3CR1$^-$ phagocytes) but not or weakly by DAV cDC2s or monocyte-derived cells (CD11c$^+$SIRPα$^+$CX3CR1$^+$ phagocytes) (Fig. 2E and Supplementary Fig. 2B). Consistent with their role in M cell maturation[20], subepithelial S100A4$^+$ cDC2s were enriched in the crypts and at the base of the dome where immature M cells are located (Fig. 2E). They also penetrated the FAE at this site. However, their number rapidly decreased in the upper part of the SED where monocyte-derived cells involved in antigen sampling became largely predominant (Fig. 2E). We next sought to identify mature cDC2s based on the expression of typical cDC maturation marker genes, such as *Ccr7* and *Cd83* (Fig. 2A and 2F). Interestingly, some genes, such as *Nudt17*, *Socs2,* and the T cell-attracting chemokine *Ccl22*, were late maturation markers as compared to *Cd83*, *Ccr7*, *Il4i1* and *Gadd45b*, which showed a broader expression pattern with an expression gradient likely reflecting the maturation pathway of cDC2s (Fig. 2F and Supplementary Fig. 2C). Other genes, such as *Rel* and *Cxcl16*, showed an even broader expression profile encompassing another cluster likely representing an intermediate state of maturation (Fig. 2A and 2F; Supplementary Fig. 2C). We have previously shown that the surface expression of CD24 decreases while that of JAM-A increases upon maturation of dome cDC2s[13]. Indeed, *F11r*, which encodes JAM-A was predominantly expressed by both intermediate and mature cDC2 clusters, whereas *Cd24a* was expressed by all cDC2s except mature ones (Fig. 2A and 2G).

The proliferative cDC2 cluster, defined by the expression of typical proliferation markers genes, such as *Birc5* and *Mcm7*, was located opposite mature cDC2s in the UMAP (Fig. 2A and 2H). This cluster and part of its two nearest neighbors expressed the transcription factor *Bcl11a*, which is required for Flt3 expression in early cDC differentiation[21] and *Cd7*, a transient marker of pre-cDCs and pre-cDC2s[22] (Fig. 2I), suggesting that these clusters are likely to contain immature cDC2s. One of these clusters enriched for *Ccr6* also specifically expressed the cadherin gene *Cdh17* (Fig. 2I). We observed cadherin 17 expression by cDC2s in the SED (Supplementary Fig. 2D). However, in the IFR, cadherin 17 was also expressed by rare, probably newly recruited, cDC2s as well as by other immune cells that did not express phagocyte markers (Supplementary Fig. 2E).

To corroborate these findings and determine the differentiation pathway of dome cDC2, we used the RNA velocity-based algorithm scVelo[23]. Clusters of dome cDC2s showed a ratio of unspliced mRNA between 22% and 27% of total mRNA, validating this approach to infer cell fate trajectories (Fig. 2J). Based on the dynamic mRNA velocity streamlines projected onto the cDC2 subclustering UMAP, the emission basins, i.e. the differentiation starting points of dome cDC2s, were located close to proliferative cDC2s (Fig. 2J). Several intermediate basins with converging streamlines on one side and emerging streamlines on the other were found, two of which were located in immature cDC2s close to the intermediate cDC2 cluster. Finally, three

Fig. 2 Transcriptional profile and differentiation pathways of dome cDC2s *in vivo*. (A) UMAP embedding map colored by Seurat clustering of 2406 cDC2s extracted from PPs shows a large group of five dome cDC2 clusters and a small isolated cluster of DAV cDC2s. Color code, identification of each cluster based on gene expression, number of cells, and percentage of total cDC2s are shown below the UMAP. (B) Projection of *Apol10b* and *Cd209b* expression onto cDC2 UMAP, highlighting the DAV cDC2 cluster. (C) Flow cytometry analysis of CD101 and CD209b expression in villus and PP CD11c enriched cells shows their expression by villus but not PP cDC2s. Dot plots are representative of three independent experiments with three C57Bl/6 mice/experiment. (D and E) Expression of S100A4 gene (D) and protein (E) in dome but not DAV cDC2s; (E) By spectral confocal microscopy, expression of S100A4 (magenta) in the SED is mainly concentrated in SIRPα$^+$ (orange), CX_3CR1^- (green), CD11c$^+$ (red) cDC2 of the first half of dome height whereas monocyte-derived cells (i.e. LysoDCs and LysoMacs, SIRPα$^+$-CX_3CR1^+CD11c$^+$ cells) are enriched in the upper part of the SED. Some S100A4$^+$ cDC2 penetrate the FAE (arrowheads). S100A4 is also expressed by small CD11c$^-$Sirpα$^-$CX3CR1$^-$ cells, presumably ILC3s, located just below the subepithelial phagocyte layer (asterisks). The image is representative of observations made on ileal PPs from more than 5 $CX3CR1^{GFP/+}$ mice. (F–I): Projection of maturation (F), differentially expressed (G), proliferation (H) and immature (I) marker gene expression on cDC2 UMAP. (J and K) mRNA velocity analysis of dome cDC2s; (J) Top: ratio of unspliced to spliced mRNA in dome cDC2 clusters. Bottom left: mRNA velocity streamlines projected onto cDC2 UMAP. Streamline emission basins are shown in purple, intermediate basins are mixed purple to red depending on streamline orientation, and streamline attraction basins are shown in red. Bottom right: latent time UMAP highlighting the main terminal differentiation state of cDC2s in yellow; (K) Heatmap of the top 150 likelihood-driver genes of cDC2 differentiation trajectories resolved along latent time. Velocity (abundance of unspliced RNA) and expression of four representative driver genes *Runx3*, *Il22ra2*, *Stat1* and *Ccr7* are shown on the right. See also Supplementary Fig. S2 for additional gene expression in cDC2s and the location of S100A4- and cadherin 17-expressing cDC2s in PPs. CD = clusters of differentiation; cDC = conventional dendritic cell; DAV = dome-associated villi; FAE = follicle-associated epithelium; GFP = green fluorescent protein; mRNA = messenger RNA; PP = Peyer's patch; SED = subepithelial dome; UMAP = uniform manifold approximation and projection.

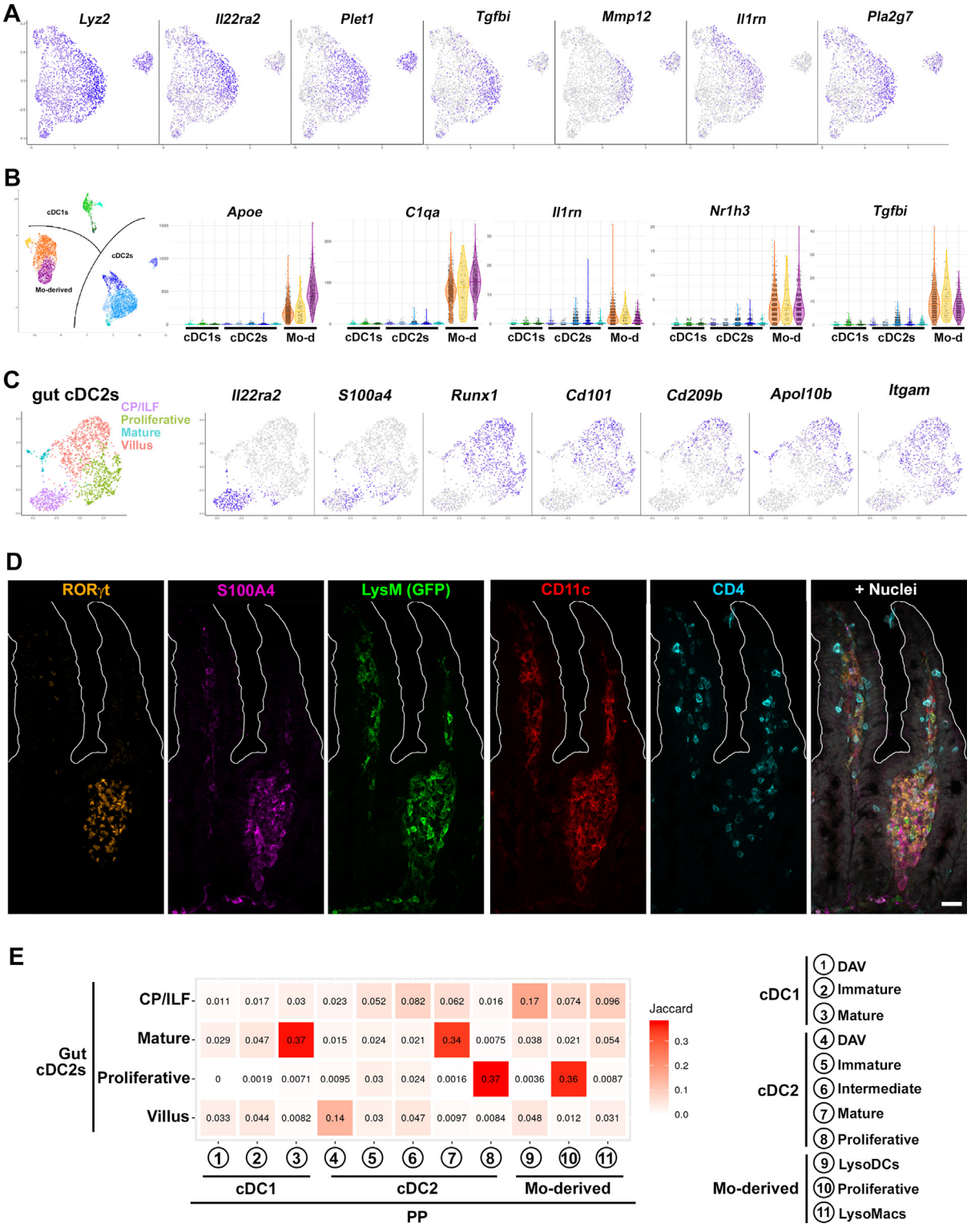
A
Lyz2
Il22ra2
Plet1
Tgfbi
Mmp12
Il1rn
Pla2g7
B
cDC1s
cDC2s
Mo-derived
Apoe
C1qa
Il1rn
Nr1h3
Tgfbi
cDC1s cDC2s Mo-d
C
gut cDC2s
CP/ILF
Proliferative
Mature
Villus
Il22ra2
S100a4
Runx1
Cd101
Cd209b
Apol10b
Itgam
D
RORγt
S100A4
LysM (GFP)
CD11c
CD4
+ Nuclei
E
Gut cDC2s
CP/ILF 0.011 0.017 0.03 0.023 0.052 0.082 0.062 0.016 0.17 0.074 0.096
Mature 0.029 0.047 0.37 0.015 0.024 0.021 0.34 0.0075 0.038 0.021 0.054
Proliferative 0 0.0019 0.0071 0.0095 0.03 0.024 0.0016 0.37 0.0036 0.36 0.0087
Villus 0.033 0.044 0.0082 0.14 0.03 0.047 0.0097 0.0084 0.048 0.012 0.031
1 2 3 4 5 6 7 8 9 10 11
cDC1
cDC2
Mo-derived
PP
Jaccard
0.3
0.2
0.1
0.0
cDC1
1 DAV
2 Immature
3 Mature
cDC2
4 DAV
5 Immature
6 Intermediate
7 Mature
8 Proliferative
Mo-derived
9 LysoDCs
10 Proliferative
11 LysoMacs

attraction basins, i.e. differentiation endpoints of dome cDC2s, were observed, suggesting that cDC2s may have different fates depending on the signals they receive from their microenvironment. Nevertheless, the transcriptional dynamics of cDC2s, displayed as latent time UMAP, highlighted the mature cDC2 cluster as the major terminal differentiation state of cDC2s (Fig. 2J). Finally, the heatmap of the top 150 likelihood-driver genes of the PP cDC2 differentiation trajectory resolved along latent time allowed us to infer the chronology of marker expression for cDC2 differentiation and maturation. It showed a clear cut in the transcriptional cascade at the boundary between the mature cDC2 cluster and the other clusters, illustrating the profound changes that occur during the maturation process (Fig. 2K). In terms of transcription factors, *Runx3* was expressed early during cDC2 differentiation, whereas *Stat1*, *Rel,* and *Nr4a3* were induced at the transitional stage of maturation. Velocity of *Ccr7* (relative abundance of unspliced RNA) peaked in the intermediate cDC2 cluster, well before reaching its highest expression in the mature cDC2 cluster, confirming the differentiation state of both intermediate and mature dome cDC2 clusters (Fig. 2K).

Gut-associated lymphoid tissue cDC2s follow a specific differentiation program

Recently, a cDC2 subset specific for cryptopatches (CPs) and isolated lymphoid follicles (ILFs) has been characterized by its expression of lysozyme M, IL22-BP, and PLET1[24]. We have previously shown that half of the CD11b$^+$ cDC2s in PP express lysozyme M[13]. To determine whether lysozyme M-expressing CD11b$^+$ dome cDC2s are similar to those present in CPs and ILFs, we examined the expression of the latter key genes in our dataset. We found that the intermediate cDC2 cluster expressing the highest levels of *Lyz2*, which encodes lysozyme M, also expressed *Il22ra2* and *Plet1* (Fig. 2K and 3A). In addition, this cluster was also enriched for other CP/ILF cDC2-specific genes, such as *Tgfbi*, *Mmp12*, *Il1rn*, and *Pla2g7* (Fig. 3A), suggesting that the specific pattern of gene expression observed in CP/ILF cDC2s can be generalized to all gut-associated lymphoid tissues (GALTs). Since some maturation markers were already expressed in the GALT-specific cDC2 cluster and some CP/ILF cDC2 specific genes, such as *Il1rn*, *Pla2g7,* and *IL22ra2* were also expressed by mature dome cDC2s (Fig. 2F and 3A; Supplementary Fig. 2C), this gene signature marked an intermediate to full maturation state of GALT cDC2s. This signature also showed strong similarities with LysoDC and LysoMac transcriptional profiles, including the expression of *Csf1r*, *Il22ra2*, *Il1rn*, *Lyz1,* and *Lyz2* but also of *Apoe*, *C1qa, Nr1h3*, *Pla2g7*, and *Tgfbi* (Fig. 3B). However, the expression of these genes was much higher in LysoDCs and LysoMacs than in GALT-specific cDC2s (Fig. 1B, 1C and 3B; Supplementary Fig. 1B). To confirm the similarity between dome and CP/ILF cDC2s, we analyzed the expression of genes highlighted in our study in the intestinal cDC2s dataset, which includes CP/ILF cDC2s[24]. Indeed, *Runx1*, *Cd101*, *Apol10b*, *Cd209b,* and *Itgam* were associated with villus cDC2s but not with CP/ILF cDC2s, whereas *S100a4* expression was associated with the CP/ILF cDC2 cluster identified by its specific expression of *Il22ra2* (Fig. 3C). S100A4 expression by ILF cDC2s was confirmed by microscopy (Fig. 3D). Finally, similarities between conventional villus and DAV cDC2s and between CP/ILF cDC2s and PP dome intermediate/mature cDC2s were confirmed by a Jaccard index (Fig. 3E). Collectively, these results suggest that GALT cDC2s follow a common maturation program that is specifically shaped by their microenvironment.

The transcriptional profile of dome cDC1s reveals the chronology of their differentiation and maturation *in vivo*

The cDC1s were divided into six clusters (Fig. 4A). One of these clusters was segregated from the others and was therefore suspected to correspond to DAV cDC1s. This cluster typically lacked expression of the transcription factor *Jun*, of the mRNA-binding protein genes *Zfp36* and *Zfp36l1*, of the long non-coding RNA *Neat1*, and of *Clec12a* (Fig. 4A and 4B). Like DAV cDC2s, putative DAV cDC1s were enriched for *Mgl2* (Fig. 4C). We confirmed by microscopy that some, but not all, CD11c$^+$ phagocytes from villi expressed MGL2, whereas dome phagocytes did not (Supplementary Fig. 3A and 3B). DAV cDC1s were also enriched for *Ctla2b* and *Dapk2*, which together with *Mgl2* were also expressed by another small cluster enriched for *Stt3b* expression (Fig. 4A and 4C).

Like mature cDC2s, mature cDC1s were located in the UMAP opposite to the proliferative cDC1 cluster (Fig. 4A and 4D). Similarly, the expression pattern of *Rel* was broader than that of *Ccr7*, *Cd83,* and *Gadd45b*, which in turn was broader than that of *Ccl22*, *Nudt17,* and *Socs2* (Fig. 4D and Supplementary Fig. 3C), confirming their status as early, intermediate and late maturation markers, respectively. However, *Cxcl16* was expressed by all cDC1s, although enriched in mature cDC1s (Supplementary Fig. 3D). *Aldh1a2*, *Glipr2,* and *Il12b*, which are involved in retinoic acid production, autophagy regulation, and T-cell polarization respectively, were enriched in mature cDC1s compared to mature cDC2s (Fig. 4E), whereas mature cDC2s, but not cDC1s, were enriched in the lipid-binding protein-encoding genes *Fabp5* and *Gpr183* (Fig. 4F).

The closest neighbor to the proliferative cDC1 cluster expressed the early cDC marker *Bcl11a*, and *Ccr2*, a transient marker of pre-cDCs and pre-cDC1s[22] (Fig. 4G). Finally, the cluster in between these immature and mature cDC1s, presumed to be

Fig. 3 Core differentiation program of gut-associated lymphoid tissue cDC2s. (A) Projection of CP/ILF cDC2 marker gene expression onto PP cDC2 UMAP shows enrichment in the intermediate to mature dome cDC2 clusters. (B) Violin plots of CP/ILF cDC2 marker genes in PP phagocyte clusters as shown on the left UMAP. In addition to moderate expression by intermediate to mature dome cDC2s, they are enriched in monocyte-derived cells. (C) Projection of the expression of some of the cDC2 markers highlighted in this study onto the intestinal cDC2 UMAP of the EBI database E-MTAB-9522 (intestinal cDCs)[24]. The expression of dome (*S100a4*) and DAV (*Runx1*, *Cd101*, *Apol10b*, *Cd209b*, and *Itgam*) specific genes are either enriched or downregulated in the *Il22ra2*$^+$ CP/ILF cDC2 cluster, respectively. (D) Location of S100A4$^+$ (magenta) CD11c$^+$ (red) LysM$^+$ (GFP, green) cDC2s in an immature ILF (RORgt-enriched region in orange) but not in adjacent villi. The image is representative of observations made on ILFs from three Lys-EGFP mice. (E) Jaccard index between the transcriptional profiles of intestinal cDC2 and PP phagocytes. CP/ILF cDC2s are closer to monocyte-derived cells and intermediate and mature dome cDC2s than to DAV cDC2s, whereas villus cDC2s are close to DAV cDC2s. cDC = conventional dendritic cell; CP = cryptopatch; DAV = dome-associated villi; GFP = green fluorescent protein; ILF = isolated lymphoid follicle; PP = Peyer's patch; UMAP = uniform manifold approximation and projection.

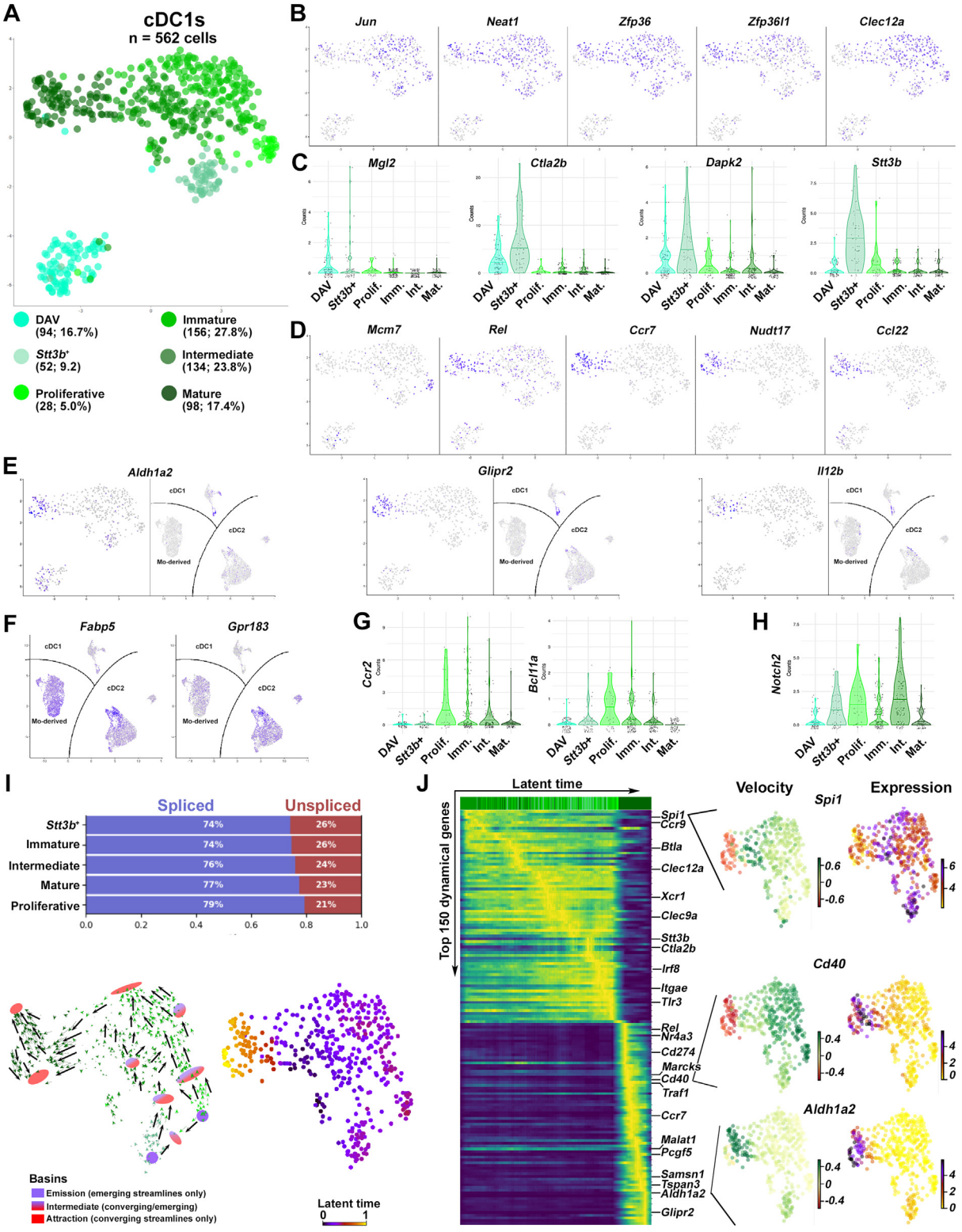
A
cDC1s
n = 562 cells
DAV (94; 16.7%)
Stt3b+ (52; 9.2)
Proliferative (28; 5.0%)
Immature (156; 27.8%)
Intermediate (134; 23.8%)
Mature (98; 17.4%)
B
Jun
Neat1
Zfp36
Zfp36l1
Clec12a
C
Mgl2
Ctla2b
Dapk2
Stt3b
DAV
Stt3b+
Prolif.
Imm.
Int.
Mat.
D
Mcm7
Rel
Ccr7
Nudt17
Ccl22
E
Aldh1a2
Glipr2
Il12b
cDC1
cDC2
Mo-derived
F
Fabp5
Gpr183
G
Ccr2
Bcl11a
H
Notch2
I
Spliced
Unspliced
Stt3b+ 74% 26%
Immature 74% 26%
Intermediate 76% 24%
Mature 77% 23%
Proliferative 79% 21%
Basins
Emission (emerging streamlines only)
Intermediate (converging/emerging)
Attraction (converging streamlines only)
Latent time
J
Latent time
Top 150 dynamical genes
Spi1
Ccr9
Btla
Clec12a
Xcr1
Clec9a
Stt3b
Ctla2b
Irf8
Itgae
Tlr3
Rel
Nr4a3
Cd274
Marcks
Cd40
Traf1
Ccr7
Malat1
Pcgf5
Samsn1
Tspan3
Aldh1a2
Glipr2
Velocity
Expression

intermediate cDC1s, was enriched for *Notch2* expression (Fig. 4H).

mRNA velocities confirmed cDC1 differentiation trajectories and identified their putative driver genes (Fig. 4I and 4J). The mature cDC1 cluster was clearly identified as the terminal differentiation state by the latent time UMAP (Fig. 4J). There was also a clear cut in the transcriptional cascade of the top 150 likelihood-driver genes at the level of the mature cDC1 cluster (Fig. 4J). Among these genes, *Cd40* was induced in immature and intermediate cDC1s well before reaching its peak of expression in mature cDC1s, whereas *Aldh1a2* was representative of late maturation markers and was restricted to mature cDC1s. Finally, the chronology of maturation marker expression obtained for both cDC1s and cDC2s identified: (i) common early maturation markers, including *Cd274* encoding the immunoregulatory molecule PD-L1, *Cd83* and the transcription factors *Rel* and *Nr4a3*; (ii) common intermediate maturation markers, such as *Ccr7, Marcks*, *Traf1* and *Gadd45b*; and (iii) common late maturation markers, including *Ccl22*, *Socs2*, *Nudt17*, the gene expression repressor *Pcgf5* and the transmembrane protein *Tspan3* (Fig. 2F, 2K, 4D, and 4J; Supplementary Figs. 2C and 4C).

Differentiation pathway analysis of monocyte-derived phagocytes reveals greater plasticity of LysoDCs compared to macrophages

LysoDCs accounted for 64.3% of the monocyte-derived cells. Approximately 6% of monocyte-derived cells were in proliferation, most of which were LysoDCs (*Cd4*$^-$ cells expressing high levels of MHCII-related genes) (Fig. 5A and 5B). Thus, both short-lived LysoDCs and cDCs, but not long-lived LysoMacs, showed marked proliferative activities in PPs. As expected, mature LysoDCs, as revealed by their *Plet1*, *Cd9,* and *Ifitm1* expression[7], were located in the UMAP opposite to proliferative LysoDCs (Fig. 5A and 5B). As previously described[7], they were enriched for *Il1b*, *F11r,* and *Cd24* expression whereas follicular LysoDCs lacked *Emb* (Fig. 5B).

In addition to *Cd4*, LysoMacs were enriched for *Tspan 10* (Fig. 5B). They were divided into two clusters, expressing or not *Timd4*, which encodes TIM4 (Fig. 5A and 5B). TIM4$^+$ LysoMacs were enriched for *Wfdc17* expression.

As previously described[7], scVelo revealed two attraction basins in mature LysoDCs and one in follicular LysoDCs (Fig. 5C). In contrast, most LysoMacs converge toward a single fate located at the edge of TIM4$^+$ LysoMacs (Fig. 5C). This was confirmed by LysoMac subclustering and latent time analysis. Consistent with the loss of macrophage mobility in the tissues, *Actb*, which encodes actin, was already downregulated in the emission basin, whereas *Timd4*, *C3*, *Clec1b*, *Igf1*, and *Vcam1* were upregulated in the most mature LysoMacs (Fig. 5D). Collectively, these results suggest that, unlike LysoDCs, LysoMacs converge on a single fate at steady state.

TLR7 and TLR9 stimulation *in vivo* alters the transcriptional profile of PP phagocytes

We next investigated the activation of PP phagocytes by TLR stimulation *in vivo*. We have previously shown that the TLR7 ligand R848 is a potent direct activator of monocyte-derived cells as well as an indirect activator of cDCs through a TNF-dependent pathway[7,13]. We decided to study their activation by another endosomal TLR with broad expression in phagocytes, TLR9. The TLR9 ligand CpG failed to induce activation of PP cDCs by oral administration, possibly due to its degradation by the acidic pH of the stomach or by nucleases in the gastrointestinal tract[25]. However, it induced cDC activation when administered intraperitoneally (Supplementary Fig. 4A). Furthermore, PP cDCs stimulated with the TLR7 ligand R848 via the oral or intraperitoneal route showed similar increases in surface expression of MHCII, CD40, CD86, and CD205 (Supplementary Figs. 4A and 4B). We, therefore, decided to continue our investigation using intraperitoneal injection for both TLR ligands. Since surface expression of co-stimulatory molecules peaks 8 hours after intraperitoneal CpG injection (Supplementary Fig. 4C) and LysoDC migration from the SED to the IFR begins 8 hours after R848 stimulation[7], we decided to perform scRNAseq analysis of PP phagocytes 9 hours after stimulation with both TLR ligands. In agreement with previous results[13], we obtained twice as many cDC1s after R848 stimulation, but the most striking difference was obtained with CpG stimulation, where three times as many cDC1s but also 1.5 times as many cDC2s were obtained (Supplementary Table 1). Thus, cDCs represented approximately 90% of the total phagocytes after CpG stimulation. Based on these phagocyte ratios, we decided to discard half of the R848-stimulated cDC2s as at steady state but also 2/3 of the cDC2s and half of the cDC1s stimulated with CpG prior to scRNA-seq library preparation (Supplementary Table 1).

Fig. 4 Transcriptional profile and differentiation pathways of dome cDC1s in vivo. (A) UMAP embedding map colored by Seurat clustering of 562 cDC1s extracted from PPs showed a large group (468 cells) of five dome cDC1 clusters and a small isolated cluster (94 cells) of DAV cDC1s. Color code, identification of each cluster based on gene expression, number of cells and percentage of total cDC1s are shown below the UMAP. (B) Projection of dome cDC1 marker gene expression onto the cDC1 UMAP. (C) Violin plots of DAV cDC1 marker gene expression in the cDC1 clusters described in (A). (D and E) Projection onto cDC1 UMAP or onto total PP phagocyte UMAP of the expression of the cell division marker *Mcm7* (DNA replication licensing factor) and cDC maturation marker genes, highlighting the proliferative and mature clusters, respectively. (F) Projection of the expression of the lipid-binding protein-coding genes *Fabp5* and *Gpr183* onto total PP phagocyte UMAP shows an enrichment in mature cDC2 but not in cDC1. (G and H) Violin plots of the pre-cDC1 markers *Ccr2* and *Bcl11a* (G) and of *Notch2* (H) in the cDC1 clusters described in (A). (I and J) mRNA velocity analysis of dome cDC1s; (I) Upper left panel: ratio of unspliced to spliced mRNA in dome cDC1 clusters. Bottom left: single-cell mRNA velocity projected onto cDC1 UMAP. Major directions are indicated by arrows and emission, intermediate and attraction basins are shown in purple, mixed purple to red and red, respectively. Bottom right: latent time UMAP highlighting the main terminal differentiation state of cDC1s in yellow; (J) Heatmap of the top 150 likelihood-driver genes of cDC1 differentiation trajectories resolved along latent time. Velocity and expression of three representative driver genes *Spi1*, *Cd40* and *Aldh1a2* are shown on the right. See also Supplementary Fig. S3 for MGL2/CD301b expression in the gut and additional gene expression in mature cDC1s. cDC = conventional dendritic cell; DAV = dome-associated villus; Imm., immature; Int., intermediate; Mat., mature; mRNA = messenger RNA; PP = Peyer's patch; prolif., proliferative; UMAP = uniform manifold approximation and projection.

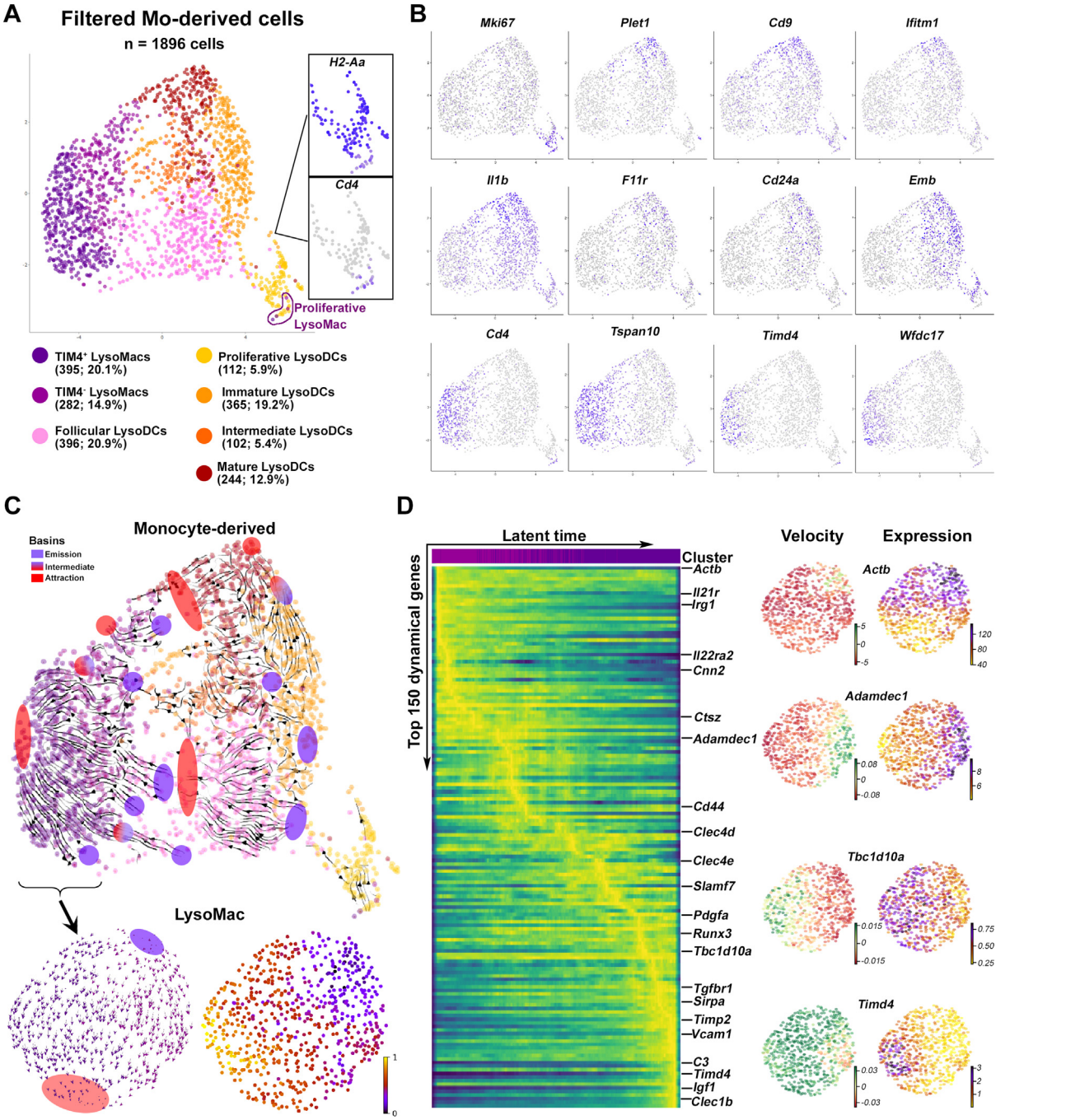

Fig. 5 Transcriptional profile and differentiation pathway of monocyte-derived phagocytes *in vivo*. (A) UMAP embedding map colored by Seurat clustering of 1896 filtered monocyte-derived phagocytes extracted from PPs shows a large group (1784 cells) of six clusters and a small peripheral cluster (112 cells) consisting mainly of proliferative LysoDC. Color code and identification of each cluster based on gene expression with the number of cells and percentage of total monocyte-derived phagocytes in brackets are shown below the UMAP. (B) Expression of genes differentially expressed between clusters. (C) mRNA velocity analysis of monocyte-derived phagocytes. Top: mRNA velocity streamlines projected onto the monocyte-derived phagocyte UMAP. Emission, intermediate, and attraction basins are shown in purple, mixed purple to red, and red, respectively. Bottom: mRNA velocity streamlines (left) and latent time UMAP (right) in subclustered LysoMac. (D) Right panel: heatmap of the top 150 likelihood-driver genes of LysoMac differentiation trajectories resolved along latent time. Velocity and expression of four representative driver genes *Actb*, *Adamdec1*, *Tbc1d10a,* and *Timd4* are shown on the right. DC = dendritic cell; mRNA = messenger RNA; PP = Peyer's patch; UMAP = uniform manifold approximation and projection.

As at steady state, cDC1s, cDC2s, and monocyte-derived cells were separated on the UMAP of R848 and CpG-activated phagocytes (Fig. 6A). Distinction between LysoDCs and LysoMacs was more pronounced than at steady state, indicating divergent activation processes for both types of monocyte-derived cells. Both TLR ligands led to a loss of *Itgax* expression encoding CD11c in

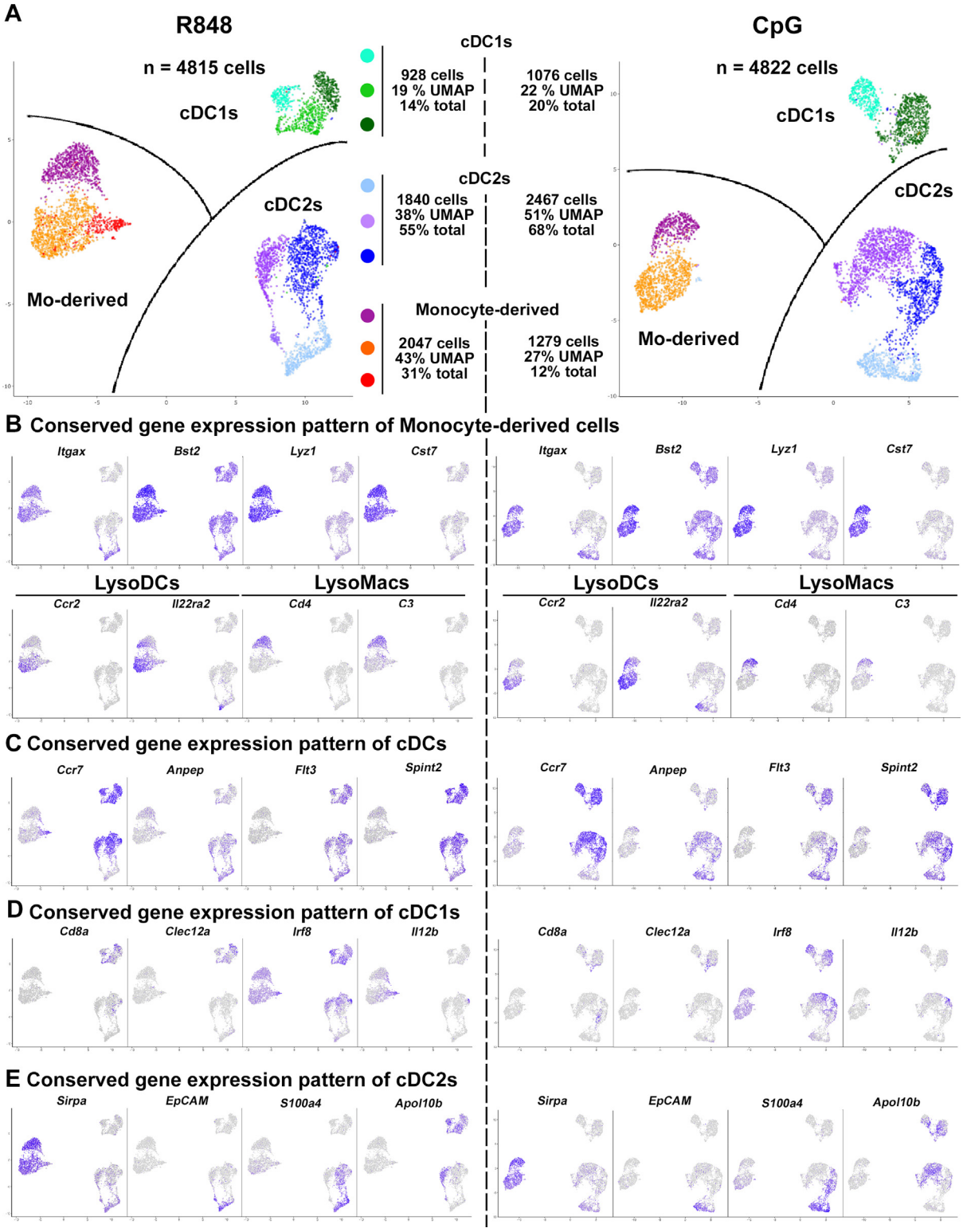
A
R848
n = 4815 cells
cDC1s
cDC2s
Mo-derived
cDC1s
928 cells
19 % UMAP
14% total
1076 cells
22 % UMAP
20% total
cDC2s
1840 cells
38% UMAP
55% total
2467 cells
51% UMAP
68% total
Monocyte-derived
2047 cells
43% UMAP
31% total
1279 cells
27% UMAP
12% total
CpG
n = 4822 cells
cDC1s
cDC2s
Mo-derived
B Conserved gene expression pattern of Monocyte-derived cells
Itgax
Bst2
Lyz1
Cst7
LysoDCs
LysoMacs
Ccr2
Il22ra2
Cd4
C3
C Conserved gene expression pattern of cDCs
Ccr7
Anpep
Flt3
Spint2
D Conserved gene expression pattern of cDC1s
Cd8a
Clec12a
Irf8
Il12b
E Conserved gene expression pattern of cDC2s
Sirpa
EpCAM
S100a4
Apol10b

most cDCs but not in monocyte-derived cells (Fig. 6B). Expression of MHCII pathway genes was also reduced in a proportion of activated cDCs, but maintained in all LysoDCs and not induced in LysoMacs (Supplementary Fig. 5A). Expression of the PP monocyte-derived cell markers *Bst2* and *Lyz1*, and the genes encoding Gas7 and the lysosomal machinery (Lamp1, Lamp2, Cystatin F and cathepsin genes) was conserved upon activation (Fig. 6B and Supplementary Fig. 5B), consistent with the preserved ability of LysoDCs to phagocytose particulate antigens after R848 stimulation[7]. However, in a small peripheral cluster of R848-stimulated LysoDCs that expressed *Ccr7*, and thus included the most activated LysoDCs, key genes of the monocytic lineage, including *Csf1r*, *Cx3cr1*, *Ccr2*, *Mafb*, and *Msr1*, were typically downregulated, with the notable exception of *Mertk* and *Lyz2* (Fig. 6B and Supplementary Fig. 5C). Finally, the expression of *Cd4* and *C3* was maintained by LysoMacs upon activation (Fig. 6B).

For cDCs, expression of the signature genes *Flt3*, and *Spint2* was maintained upon activation, whereas *Anpep* was lost in cDC1s (Fig. 6C). *Ccr7*, *Gpr132*, *Hmg3,* and *P2ry10* were highly expressed as compared to steady state (Fig. 6C and Supplementary Fig. 5D for comparison with Supplementary Fig. 1D).

Most cDC1s marker genes were repressed upon activation with the notable exception of *Cd8a* and *Clec12a* for R848 stimulation and of *Irf8* for both stimuli (Fig. 6D). Actually, *Irf8* was expressed by all activated phagocytes. Interestingly, *Il12b*, which is mainly expressed by mature cDC1s at homeostasis, was repressed in activated cDC1s in both stimulation conditions, but induced in fully R848-activated LysoDCs and in a small cluster of activated cDC2s (Fig. 6D).

As with cDC1s, most cDC2 markers, including *Sirpa*, *Epcam,* and GALT-specific cDC2 markers, were repressed upon activation (Fig. 6E and Supplementary Figs. 5C and 5E). A cDC2 cluster that still expressed *Itgax* and the immature cDC2 markers *Bcl11a* and *Cd7*, did not express *Ccr7*, likely representing newly recruited cDC2s (Fig. 6B and 6C; Supplementary Fig. 5E). Nevertheless, expression of *S100a4* was maintained after activation in all but one cDC2 cluster (Fig. 6E). In contrast, the latter was positive for the DAV cDC2 marker gene *Apol10b* (Fig. 6E). Therefore, *S100a4* and *Apol10b* are markers of GALT cDC2 and villus cDC2, respectively, both at steady state and upon activation.

Activation profiles of monocyte-derived cells stimulated with TLR7 and TLR9 *in vivo*

Subclustering of activated monocyte-derived cells identified two clusters of LysoMacs as in steady state (Fig. 7A). However, this did not correlate with *Timd4* expression, but rather with the activation status of LysoMacs and the expression of *Ccl3*, *Ccl4,* and *Cxcl10* (Fig. 7B). Interestingly, the activation profile of follicular LysoDCs was close to that of LysoMacs (Fig. 7B). All activated monocyte-derived cells also expressed high levels of *Cxcl9* in R848-treated mice (Fig. 7B). Proliferating LysoDCs were still present after R848 treatment but not after CpG stimulation (Fig. 7A). Subepithelial LysoDCs were identified by their *Emb* expression (Fig. 7C). They also expressed the highest levels of *Ccr2* and *Il22ra2* (Fig. 7C). A proportion of them also expressed *Cd9* and *Plet1*, suggesting that, in addition to their activation process, subepithelial LysoDCs continue to follow the same differentiation pathway from immature (*Emb*$^{+}$*Plet1*$^{-}$*Cd9*$^{-}$) to mature (*Emb*$^{+}$*Plet1*$^{+}$*Cd9*$^{+}$). Consistent with previous work[6,7], fully R848-activated LysoDCs (22.2% of LysoDCs) expressed *Ccr7*, *Cd40*, *Il12b,* and *Il6* (Fig. 7D). Although not identified as such on the global phagocyte UMAP, a small cluster of *Ccr7*$^{+}$ LysoDCs (9.1% of LysoDCs) expressing *Cd40,* weak *Il6* but no *Il12b* was detected in CpG-stimulated mice (Fig. 7A and 7D).

The initial location of cDCs influences their activation profile

S100a4 and *Apol10b* expression identified dome and DAV cDC2s in the activated cDC2 subclustering (Fig. 8A). Another apolipoprotein L gene, *Apol7c*, was enriched in DAV cDC2s as compared to dome cDC2s (Fig. 8B). Newly recruited cDC2s (*Ccr7*$^{-}$ *Itgax*$^{+}$ cells) included mostly immature *Ccr6*$^{+}$ dome cDC2s (*S100a4*$^{+}$ *Apol10b*$^{-}$ cells) expressing *Runx3* with two distinct groups based on *Cdh17* and *Il22ra2* expression (Fig. 8B). R848-stimulated PPs also had a small *Ccr7* and *Ccr6* double negative cluster of immature DAV cDC2s (*S100a4*$^{-}$ *Apol10b*$^{+}$ cells) expressing *Runx1* and *Cd209b* (Fig. 8B). Instead, all DAV cDC2 clusters were *Ccr7*$^{+}$ and thus activated with CpG. We analyzed the activation profile of dome and DAV cDC2s, both of which migrate to the IFR upon activation instead of the MLNs[7,13]. *Ccl17*, *Ddt* (encoding the cytokine MIF-2/DDT), and *Ido1* were mainly expressed by activated DAV cDC2s (Fig. 8C). In contrast, activated dome cDC2s expressed the transcription factor *Tcf7*, the ICOS ligand *Icosl* and, for the most activated, *Il12b* (Fig. 8D). *Il6* expression was restricted to dome cDC2s upon R848 treatment, but extended to all activated DAV cDC2s upon CpG stimulation. We confirmed by microscopy that among phagocytes, TCF7 was mainly expressed by dome cDC2s 8 hours after R848 stimulation (Fig. 8E). Therefore, dome and DAV cDC2s have distinct activation programs, which could be due either to imprinting by their initial site of residence, i.e. villus versus dome, or to distinct migratory niches within the IFRs that provide different cues to emigrated cDC2s. To distinguish between these two possibilities,

Fig. 6 Single-cell RNA sequence analysis of R848 and CpG-stimulated PP phagocytes. (A–F) Single-cell RNA sequence analysis of 4815 and 4822 PP CD11c^{hi} phagocytes extracted from 12 C57Bl/6 mice 9 hours after intraperitoneal injection of R848 or CpG, respectively. (A) UMAP embedding map colored by Seurat clustering shows for each stimulation condition (R848 on the left; CpG on the right) three groups of clusters representing monocyte-derived cells (Mo-derived; yellow, orange and magenta clusters), cDC1s (shades of green) and cDC2s (shades of blue). The number of cells for each type of phagocytes is given in the middle column, as well as the ratio it represents in the UMAP and in the total phagocytes, considering that half of the cDC2s were discarded in the R848-treated mice and that only one-third of the cDC2s and half of the cDC1s were retained in the CpG-treated mice. (B–E) Projection of the expression of monocyte-derived cell, LysoDC and LysoMac (B), cDC (C), cDC1 (D), and cDC2 (E) marker genes onto stimulated PP phagocyte UMAPs for each stimulation condition (R848 on the left; CpG on the right) shows the transcriptional specificities of each phagocyte subset. See also Supplementary Fig. S4 for R848- and CpG-induced stimulation profiles of cDC1s and cDC2s and Supplementary Fig. S5 for additional gene expression in activated PP phagocytes. cDC = conventional dendritic cell; Mo = monocyte; PP = Peyer's patch; UMAP = uniform manifold approximation and projection.

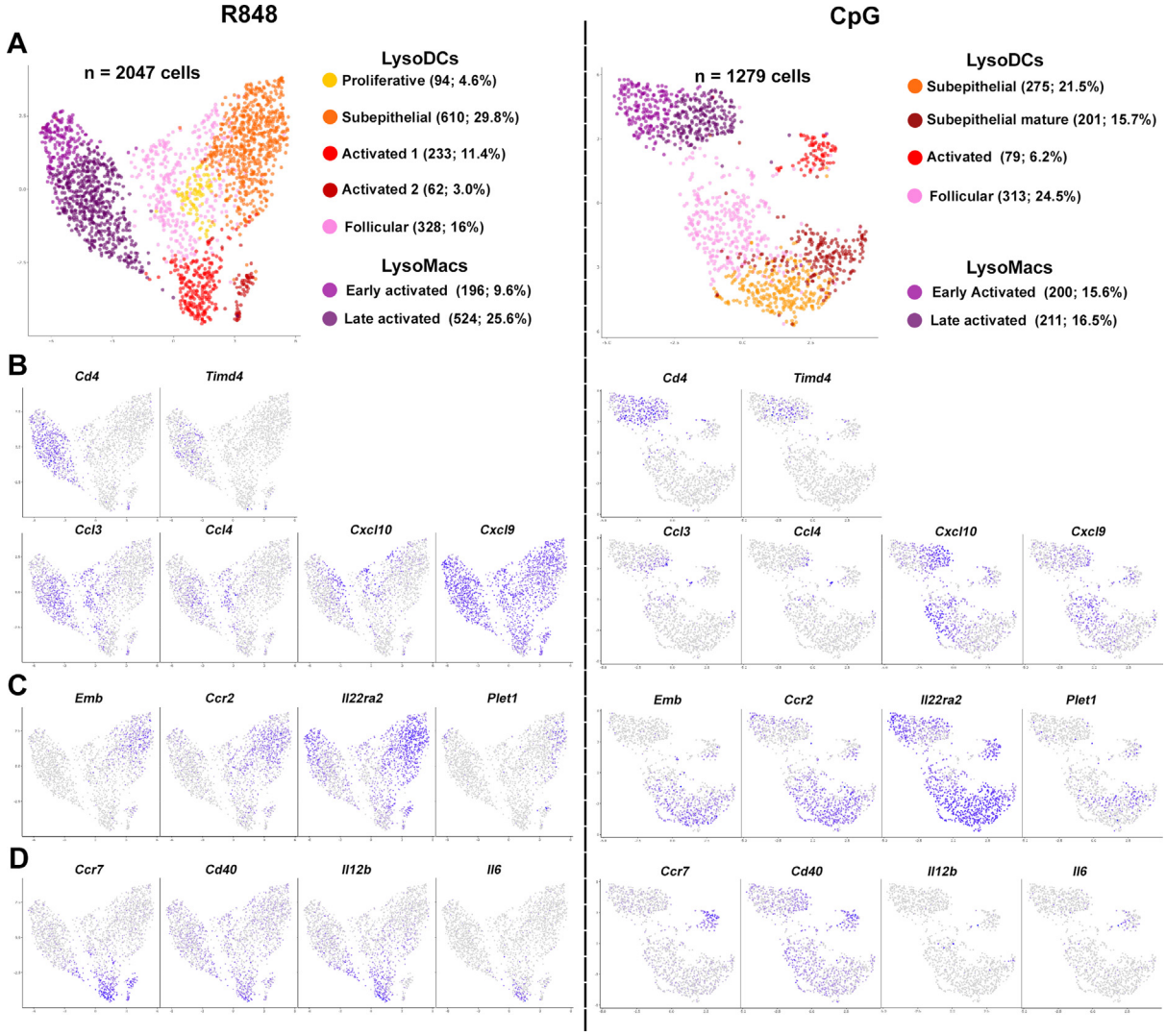

Fig. 7 Single-cell RNA sequence analysis of monocyte-derived phagocytes from R848 and CpG-stimulated PPs. (A) UMAP embedding map colored by Seurat clustering of 2047 and 1279 monocyte-derived phagocytes extracted from PPs of R848 and CpG-treated mice, respectively. Color code and identification of each cluster based on gene expression, with the number of cells and percentage of total monocyte-derived phagocytes indicated in brackets are shown on the right of each UMAP. (B–D) Projection of the expression of genes differentially expressed between clusters onto the UMAPs of stimulated monocyte-derived cells for each condition (left, R848 and right, CpG). DC = dendritic cell; PP = Peyer's patch; UMAP = uniform manifold approximation and projection.

we took advantage of the conserved expression of CD101 on the surface of emigrated DAV cDC2s[13] and of S100A4 on the surface of emigrated dome cDC2s to study their localization within the IFRs. Not only did emigrated cDC2s from both sites localized to the same sites, but they also clustered together (Fig. 9A), suggesting that their distinct activation profile is mainly due to initial niche imprinting. This clustering of DAV and dome cDC2s in the IFRs was observed from 8 to 24 hours after R848 stimulation, before $CD101^+$ cDC2 disappearance between 24 and 48 hours (Fig. 9B). Indeed, before 8 hours and after 48 hours of stimulation, the $CD101^+$ area in the IFR represented less than 5% including helper T cells ($CD4^+SIRP\alpha^-$ cells; data not shown) and was significantly lower than the $S100A4^+$ area (8.7 -/+ 3.9% of the IFR area), whereas between 8 and 24 hours the $CD101^+$ area reached 8.2 -/+ 3.9% of the IFR area and was not significantly different from the $S100A4^+$ area (Fig. 9C). Therefore, the estimated residence time of activated DAV cDC2 in the IFRs was between 16 and 40 hours post-stimulation.

Like cDC2s, cDC1s were divided into two branches, probably corresponding to activated dome and DAV cDC1s (Supplementary Fig. 6A). Thus, like activated DAV cDC2s, activated DAV cDC1s migrate to the IFRs instead of the MLNs. Since activation induced a loss of all DAV cDC1 markers, we analyzed genes that were only expressed by dome cDC1s at steady state. We found that *Jun, Neat1, Zfp36, and Zfp36l1* for both stimuli and *Clec12a* for R848 were only expressed by one of the two branches (Supplementary Fig. 6B). Therefore, even though DAV cDC1s lost their transcriptional identity upon activation and migration into IFRs, they did not acquire the gene signature of dome cDC1s.

Taken together, these data show that the initial location of intestinal cDCs influences their future activation profile in their region of emigration.

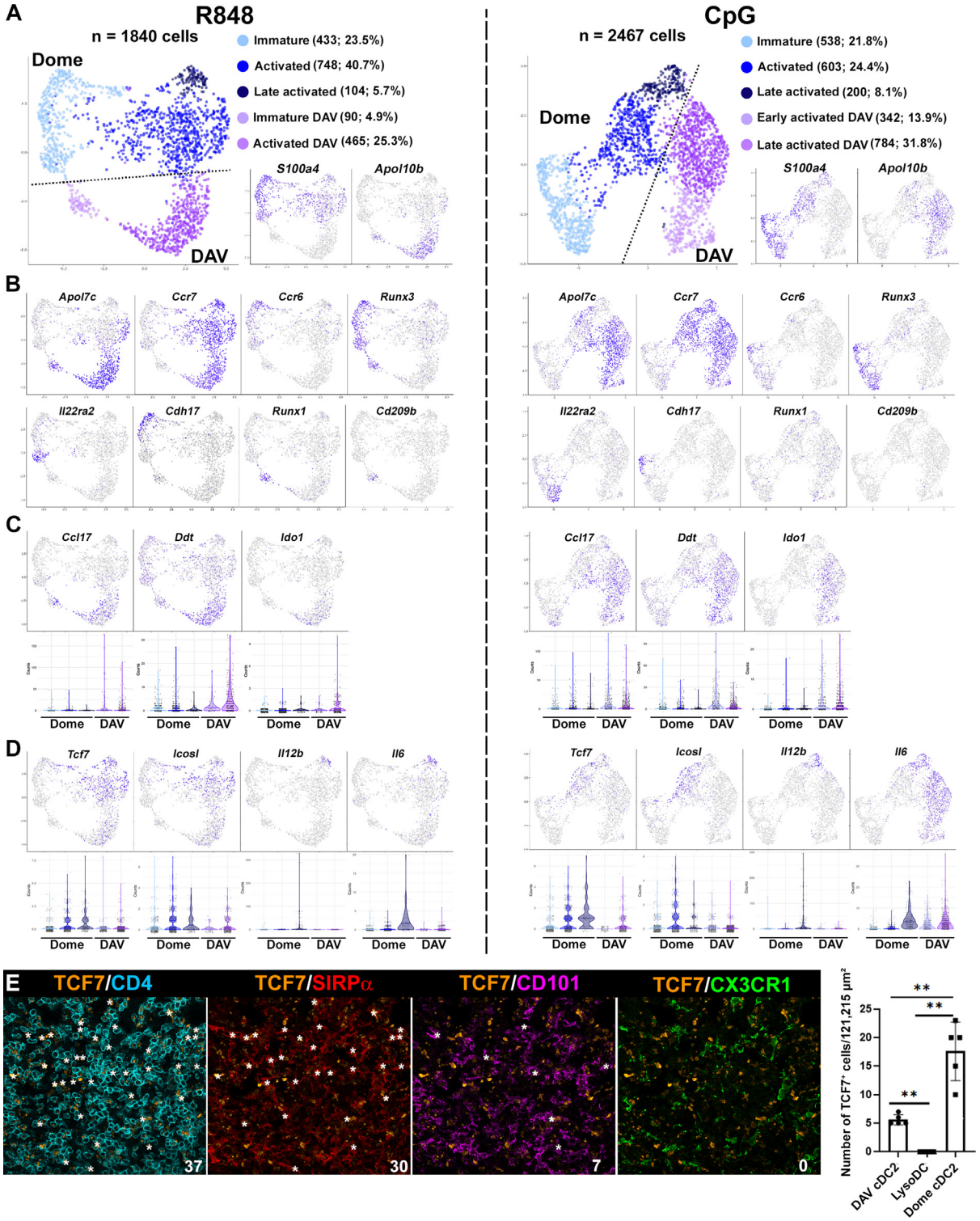
A
R848
n = 1840 cells
Immature (433; 23.5%)
Activated (748; 40.7%)
Late activated (104; 5.7%)
Immature DAV (90; 4.9%)
Activated DAV (465; 25.3%)
Dome
DAV
S100a4
Apol10b
CpG
n = 2467 cells
Immature (538; 21.8%)
Activated (603; 24.4%)
Late activated (200; 8.1%)
Early activated DAV (342; 13.9%)
Late activated DAV (784; 31.8%)
B
Apol7c
Ccr7
Ccr6
Runx3
Il22ra2
Cdh17
Runx1
Cd209b
C
Ccl17
Ddt
Ido1
Dome
DAV
D
Tcf7
Icosl
Il12b
Il6
E
TCF7/CD4
TCF7/SIRPα
TCF7/CD101
TCF7/CX3CR1
37
30
7
0
Number of TCF7+ cells/121,215 µm²
DAV cDC2
LysoDC
Dome cDC2

B and T-cell activation profiles are different in the PP of R848 and CpG-treated mice

PP DCs are involved in T-cell priming and B cell activation for IgA production[26–29]. To determine the possible consequences of the different activation profiles of PP DCs in R848- and CpG-stimulated mice on the initiation of the immune response, we analyzed the number and phenotype of B and T cells in PPs at different time points after stimulation (Supplementary Fig. 7 for gating strategies). After a slight initial increase, the number of total and naïve B cells (IgD^+ B cells) dropped below basal levels from 3 days to more than one week after stimulation with both TLR ligands (Fig. 10A). In addition, the numbers of both $CD4^+$ and $CD8^+$ naïve T cells were reduced in CpG-treated mice from 48 hours onwards. These data suggest that stimulated B and T cells rapidly exit the PP to reach effector sites. We, therefore, blocked sphingosine 1-phosphate-dependent egress from PP with FTY720 to examine activated B and T cells 72 hours after both stimulations. In CpG-treated mice, the number of activated $CD8^+$ T cells (proliferative, early and late activated) increased (Fig. 10B), in line with the strong increase in activated cDC1 numbers (Fig. 6A). In contrast, only proliferative regulatory T cells (Tregs) numbers increased in R848-treated mice (Fig. 10B). By microscopy, we indeed observed an increase in $FoxP3^+$ $CD4^+$ T cells in the SED of R848-treated mice as compared to control or CpG-treated mice (Fig. 10C). In addition, R848-treated mice showed an increase in IgA-producing B cells and, more generally, proliferative B cells (Fig. 10D). This increase was largely due to the proliferation of $CCR6^+$ B cells (Fig. 10E), which are known to be mainly located in the SED[28].

DISCUSSION

In this study, we performed a single-cell transcriptional combined with spatiotemporal analysis of PP phagocytes at steady state and upon TLR7 and TLR9 stimulation *in vivo* to decipher their maturation and activation pathways (see Supplementary Fig. 8 for a graphical summary of the main results).

To date, LysoDCs are the closest monocyte-derived cells to cDCs in mice at steady state, providing an unparalleled tool for defining the specific genetic characteristics of cDCs and monocyte-derived DCs. Surprisingly, CD26, one of the most recently identified cDC markers[18,19], failed to discriminate cDCs from monocyte-derived cells in PP. We also confirmed previous work showing that CD64, a widely used marker of monocyte-derived cells[30], is not expressed by PP monocyte-derived cells[14,31]. Both examples demonstrate the ability of the PP microenvironment to profoundly influence the phenotype of intestinal phagocytes and how delicate generalization can be. Indeed, of the initial cDC gene signature proposed by Miller *et al.*[17], only 17 genes show specificity for cDCs as compared to LysoDCs, but only two genes, *Flt3* and *Spint2*, are specifically expressed by all PP cDCs regardless of their maturation and activation state. *Flt3* is undoubtedly a key cDC marker as it is not required for the differentiation of monocyte-derived cells but is essential for the development of steady-state cDC[32,33]. In contrast, the role of *Spint2*, which encodes the serine protease inhibitor hepatocyte growth factor activator inhibitor-2 (HAI-2), is unknown. In the gut, HAI-2 expression by intestinal epithelial cells is required to inactivate the enzyme matriptase and thereby stabilize EpCAM to prevent luminal bleeding, villous atrophy, and loss of crypt architecture[34,35]. Whether HAI-2 expression in cDCs helps to prevent degradation of cell adhesion molecules deserves further investigation. Finally, the two phagocyte subsets that are the most difficult to distinguish phenotypically are derived from different precursors, monocytes for LysoDCs and the common DC precursor for dome cDC2s. However, some typical monocyte-derived cell markers, in particular MerTK and CX3CR1, are specifically expressed by LysoDCs[7,31] and can be used to distinguish them from dome cDC2s, whereas EpCAM expression, a marker of dome cDC2 maturation[13], is restricted to cDC2s.

While dome cDC2s are distinct from villus cDC2s as evidenced by their lack of CD101 and low levels of CD11b expression[13], they appear to be similar to the recently described CP/ILF cDC2s[24], bringing all GALT cDC2s together under a single banner. Thus, the key dome cDC2 marker that we have highlighted in this study, S100A4, is also expressed by CP/ILF cDC2s. S100A4 expression in the SED was initially attributed to LysoDCs, LysoMacs, and ILC3s[20]. The strong phenotypic and genetic similarity between LysoDCs and cDC2s, combined with the fact that LysoDCs do express minimal levels of S100A4 (Fig. 1F) is likely to explain the initial confusion between these two types of phagocytes. S100A4 is essential for the development of mature

Fig. 8 Single-cell RNA sequence of R848 and CpG-stimulated PP cDC2s. (A) UMAP embedding map colored by Seurat clustering of 1840 and 2467 cDC2s extracted from PPs of R848 (left) and CpG (right)-treated mice, respectively. Color code and identification of each cluster based on gene expression with the number of cells and percentage of total cDC2s indicated in brackets are shown on the upper right of each UMAP. In both conditions, two DAV cDC2 and three dome cDC2 clusters at different states of activation were obtained (dotted line in UMAPs). *S100a4* and *Apol10b* allowed to distinguish DAV from dome cDC2s (lower right). (B) Projection onto stimulated cDC2s UMAPs (left, R848 and right, CpG) of the expression of genes differentially expressed between clusters in both conditions. In both stimulation conditions, a cluster of likely newly recruited dome cDC2s was not activated (*Ccr7* negative) and represented more than 20% of total cDC2s. (C and D) Projections onto stimulated cDC2s UMAPs (upper rows) and violin plots (lower rows) of genes differentially expressed between activated DAV (C) and dome (D) cDC2s. (E) Spectral confocal imaging of TCF7 expression (orange) in the IFR of a $CX3CR1^{GFP/+}$ mouse stimulated with R848 for 8 hours. The number of $TCF7^+$ cells that did not express CD4 (asterisks, first panel) but express SIRPα (asterisks, second panel) and CD101 (asterisks, third panel) or CX3CR1 (asterisks, fourth panel) is indicated on the lower right of each panel. The number of dome cDC2s expressing TCF7 can be deduced as $SIRPα^+$ but $CD101^-$ and $CX3CR1^-$ phagocytes. Right histogram: quantification of TCF7-expressing DAV and dome cDC2s and LysoDCs in IFRs of R848-stimulated $CX3CR1^{GFP/+}$ mice. Two to three IFRs of ileal PPs were quantified per mouse from two independent experiments. Bars, 20 µm. See also Supplementary Fig. S6 for single-cell RNA sequence analysis of R848 and CpG-stimulated cDC1s. cDC = conventional dendritic cell; DAV = dome-associated villus; GFP = green fluorescent protein; IFR = interfollicular region; PP = Peyer's patch; UMAP = uniform manifold approximation and projection.

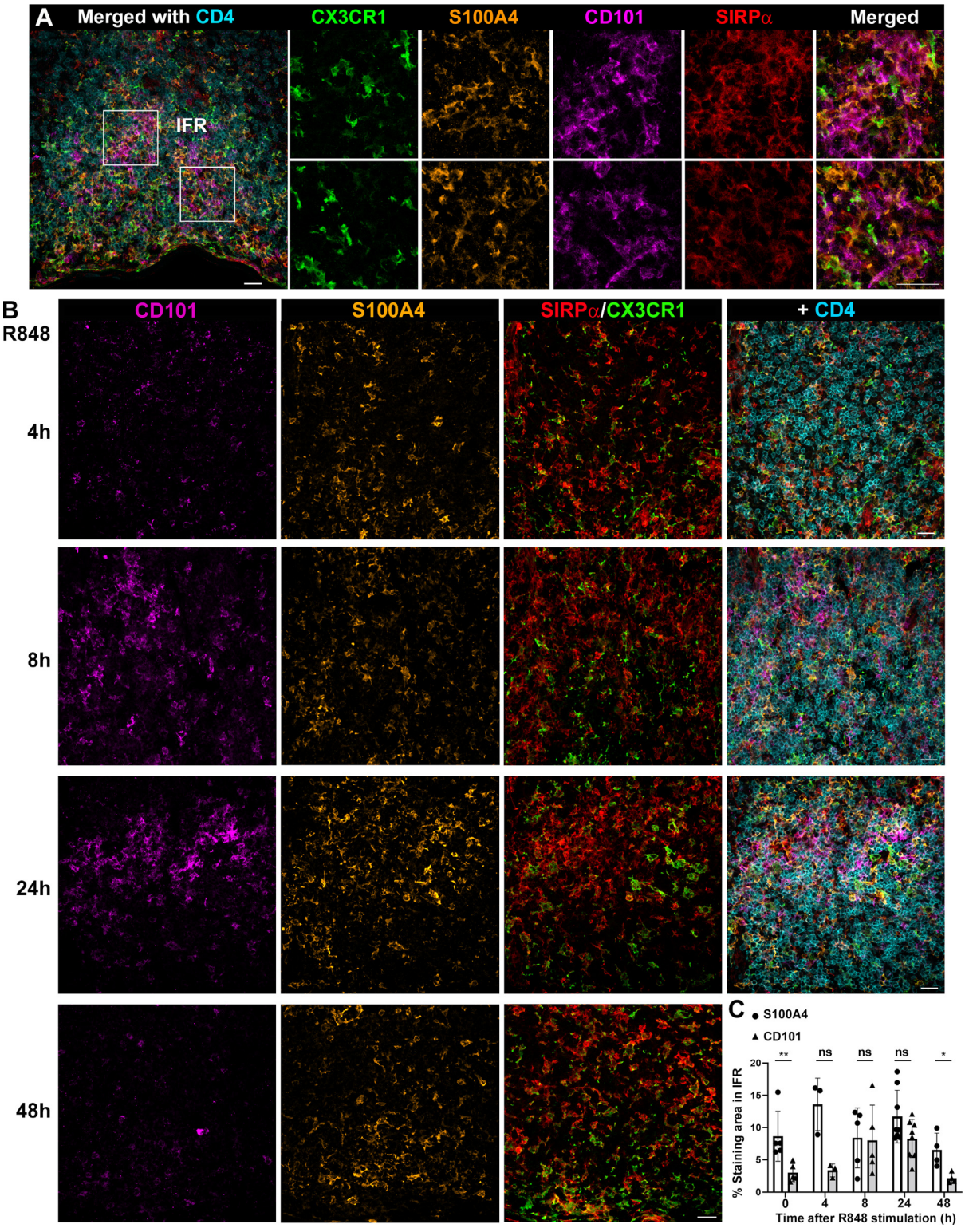
A
Merged with CD4
CX3CR1
S100A4
CD101
SIRPα
Merged
IFR
B
R848
CD101
S100A4
SIRPα/CX3CR1
+ CD4
4h
8h
24h
48h
C
S100A4
CD101
% Staining area in IFR
Time after R848 stimulation (h)
**
ns
ns
ns
*
0
4
8
24
48

M cells capable of transporting antigens[20]. In line with this, we found that subepithelial S100A4-expressing cDC2s are mainly located in the crypts and in the first half of the SED height, where they strongly interact and penetrate into the FAE at the site where M cell maturation is known to occur[36]. Regarding ILC3s, we did indeed detect S100A4 expression by small CD11c$^-$SIRPα$^-$CX$_3$CR1$^-$cells below the layer of subepithelial phagocytes but not in contact with the FAE (Fig. 2E), making their role in M cell maturation unlikely when cDC2s are present. However, they could be involved in subepithelial cDC2s programming, as it occurs in ILFs[24]. Therefore, we can propose a model in which CCR6$^+$ ILC3s of the SED would program newly recruited CCR6$^+$ subepithelial cDC2s, which in turn would induce M cell maturation by expressing S100A4.

After their initial imprinting by the GALT microenvironment, both dome cDC1s and cDC2s follow a common maturation timeline with an initial upregulation of genes encoding the transcription factors NF-kB (*Rel*) and NR4A3 (Supplementary Fig. 8). The latter has recently been shown to be involved in cDC migration by promoting the expression of *Ccr7*[37], which is actually transcribed later in the cDC maturation timeline we have established (Supplementary Fig. 8).

As expected, stimulation of PP with either of the TLR ligands R848 and CpG induces a dramatic change in the phagocyte transcriptional profile, close to, but distinct from, the steady-state mature phagocytes. Thus, while mature cDC1s express *Il12b*, activated cDC1s do not. In contrast, only R848-activated but not mature or CpG-activated LysoDCs express *Il12b* (Supplementary Fig. 8). This is in line with two previous studies showing the ability of R848-stimulated LysoDCs to induce T helper 1 polarization of naïve helper T cells *in vitro*[6] and the expression of IL-12 p40 by activated LysoDC migrating into the IFR[7].

We have shown that the site of initial residence is critical in shaping the activation profile of intestinal cDCs (Supplementary Fig. 8). Since sampling of pathogens is favored in the FAE and SED compared to the villus epithelium[4,16], this could help the immune system to locally discriminate between innocuous and harmful antigens depending on the initial site of cDCs, which could additionally provide either inflammatory (e.g. IL-6 and IL-12) or anti-inflammatory signals (e.g. kynurenines via IDO1) necessary to adequately polarize naïve T cells. Finally, differences in phagocyte activation profiles for each stimulus correlate with different adaptive immune responses, CpG favoring CD8$^+$ T-cell responses in line with the strong recruitment of cDC1s, and R848 favoring Tregs and IgA-secreting B cells. While T-cell responses require PP DCs[29], the generation of IgA-secreting B cells may involve several immune pathways, including direct activation by R848[38,39], activation by Tregs[40–42], and/or subepithelial DC[28]. Whether the increased proportion of activated LysoDCs in R848-treated mice contributes to this humoral immune response requires further investigation. In conclusion, the pathways of maturation and activation highlighted in this study open an avenue for a detailed understanding of the mechanisms involved in the initiation of the intestinal adaptive immune response.

MATERIALS AND METHODS

Mice

7–10 weeks old C57Bl6/Rj females were obtained from Janvier Labs (Le Genest Saint Isle, France). CX3CR1-GFP and Lys-EGFP mice have been previously described[43,44]. Mice were maintained at our animal house facility in ventilated cages under specific pathogen-free conditions at an ambient temperature of 22 °C with a 12-hour light/dark cycle. All experiments were done in agreement with French and European guidelines for animal care and approved by the French ethical committee.

Antibodies

XCR1-BV421 (clone ZET), CD19-BV625 (clone 6D5), BST2-PE and-BV605 (clone 927), CD11c-PE/Cy7 (clone N418), CD11b-APC/Cy7 (clone M1/70), IgD-PE/Cy7 (clone 11-26c.2a), CD8a-AF488 (clone 53–6.7), CD64-PE (clone X54-5/7.1), CD86-PE (clone GL1), CD40-biotin (clone 3/23), CD205-APC (clone NLCD-145) and CD19-BV605 (clone 6D5) were purchased from BioLegend (San Diego, CA, USA). CD24-BV786 (clone M1/69), CD172a-FITC (clone P84), CD101-AF647 (clone 307707), CCR7-PE (clone 4B12), CCR6-BV605 (29-2L17), CD45-BUV395 (clone 30-F11), Siglec-F-BV421 (clone E50-2440), PD-1-BV605 (clone J43), CD62L-PE (clone MEL-14), B220-BV786 (clone RA3-6B2), CD26-BUV737 (clone H194-112), CD43-BUV737 (clone S7), CD69-BV786 (clone H1.2F3) and BCL6-APC/Cy7 (clone K112-91) were purchased from BD Biosciences (San Jose, CA, USA). CD4-eFluor450 (clone RM4-5), Ki-67-eFluor660 and –PE/Cy7 (clone SolA15), RORgt-PE-eFluor610 (clone B2D), GL-7-eFluor660 (clone GL-7), CD3-eFluor450 (clone 17A2), CD4-PE/Cy5.5 (clone RM4-5), MHCII-A700 (clone M5/114.15.2), CD172a -biotin (clone P84), IgA-PE (clone mA-6E1), CD38-A700 (clone 90), IgM-biotin (clone II/41), FoxP3-APC (clone FJK-16S), CD44-A700 (clone IM7) and CD209b-A488 (clone 22D1) were purchased from ThermoFisher Scientific (Waltham, MA, USA).

Chicken anti-GFP (polyclonal) was from AvesLab (Davis, CA, USA). Armenian hamster anti-CD11c (clone N418) was from

Fig. 9 Kinetics of recruitment and disappearance of DAV cDC2 in the IFR of R848-treated mice. (A) Spectral confocal imaging of activated migratory DAV (CD101$^+$ and SIRPα$^+$ cells, magenta and red, respectively) and dome (S100A4$^+$ and SIRPα$^+$ cells, orange and red, respectively) cDC2s clustered together in the IFR enriched in CD4$^+$ (cyan) T cells of a CX3CR1$^{GFP/+}$ mouse stimulated with R848 for 16 hours. Monocyte-derived cells (CX3CR1$^+$ and SIRPα$^+$ cells, green and red, respectively) were also present. A higher magnification of the two boxes with individual staining display is shown on the right. (B) Spectral confocal imaging of IFRs 4 hours, 8 hours, 24 hours, and 48 hours after R848 intraperitoneal injection to CX3CR1$^{GFP/+}$ mice. Among cDC2 stained with SIRPα (red) but not CX$_3$CR1 (green), DAV cDC2 stained with CD101 (magenta) and dome cDC2 stained with S100A4 (orange) clustered together in the IFR enriched in helper T cells stained with CD4 (cyan). DAV cDC2 were recruited in the IFR from 8 to 24 hours and disappeared before 48 hours post-injection. (C) Quantification of CD101$^+$ and S100A4$^+$ area in 50,000 μm^2 area of IFRs. Smaller IFRs were not quantified. Data are representative of two (4 hours stimulation) to three (0, 8, 24, and 48 hours stimulation) independent experiments with staining of three ileal Peyer's patches/experiment. Bars, 20 μm. cDC = conventional dendritic cell; DAV = dome-associated villus; GFP = green fluorescent protein; IFR = interfollicular region; ns = not significant.

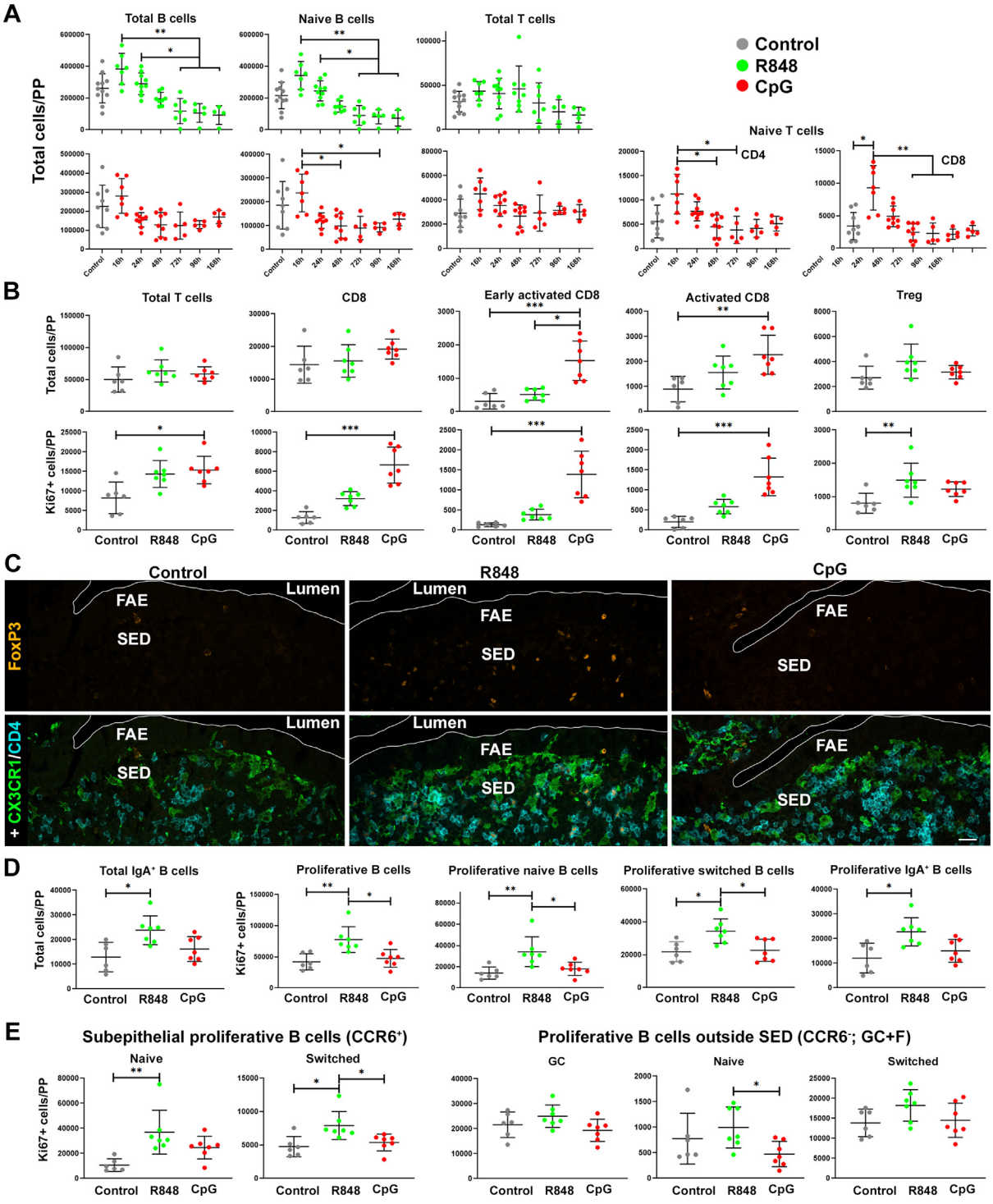

Fig. 10 B and T-cell activation profiles in PP of R848 and CpG-treated mice. (A) Kinetics of B and T cell absolute numbers in PP following treatment with R848 (top, green dots) or CpG (bottom, red dots). (B) Total (top) and proliferative (bottom) absolute numbers of T-cell subsets in PP 72 hours after R848 (green dots) or CpG (red dots) stimulation with addition of FTY720 24 hours after the stimulation. Each point (mean ± SD) represents one mouse (n ≥ 6) from three independent experiments. (C) Spectral confocal imaging of FoxP3^{+}CD4^{+} T cells accumulating in the SED of R848-treated CX3CR1$^{GFP/+}$ mice as compared to none-treated or CpG-treated mice. Representative image of two independent experiments. (D and E) B cell subset absolute numbers in PP 72 hours after R848 (green dots) or CpG (red dots) stimulation with addition of FTY720 24 hours after the stimulation. Each point (mean ± SD) represents one mouse (n ≥ 6) from three independent experiments. See also Supplementary Fig. S7 for B and T-cell subset gating strategies. FAE = follicle-associated epithelium; GFP = green fluorescent protein; Ig = immunoglobulin; PP = Peyer's patch; SED = subepithelial dome; SD = standard deviation; Treg = regulatory T cell.

BioLegend (San Diego, CA, USA). Rat anti-SIRPα (clone P84) was from BD Biosciences (San Jose, CA, USA). Rat anti-RORgt (clone AFKJS-9) was from ThermoFisher Scientific (Waltham, MA, USA). Rabbit anti-S100A4 was from Bio-Techne (Minneapolis, MN, USA). Rabbit anti-TCF7 (clone C63D9) was from Cell Signaling Technologies (Danvers, MA, USA). Donkey anti-chicken coupled to Alexa Fluor 488, goat anti-hamster coupled to Alexa Fluor 594, and donkey anti-rat coupled to Cy3 were from Jackson Immunoresearch (West Grove, PA, USA). Donkey anti-rabbit coupled to Alexa Fluor 647 and SYTOX blue were from ThermoFisher Scientific (Waltham, MA, USA).

Treatments

Gavage and intraperitoneal injections were performed with 10 µg of R848 (Invivogen, San Diego, CA, USA)) and 125 µg of CpG (Integrated DNA Technologies, Coralville, IA, USA) in 100 µl of sterile phosphate buffer saline (PBS). Fingolimod hydrochloride (FTY720, Cayman chemical company, Ann Arbor, MI, USA) was dissolved in 0.1% NaCl and injected intraperitoneally at 1 mg/kg in 200 µl 24 hours after stimulation.

Immunofluorescence staining and confocal microscopy

PP were excised and fixed with Antigenfix (Diapath, Martinengo, Italy) for 1 hour at 4 °C, washed, and incubated overnight in 30% sucrose in PBS before embedding in Tissue-Tek® Optimal Cutting Temperature (O.C.T) cryo embedding compound (Sakura Finetek Europe, Alphen aan den Rijn, The Netherlands), freezing, and storage at −20 °C. Sections were cut at 20 µm thickness and stored at −20 °C. After permeabilization and unspecific binding site blocking with PBS containing 0.5% saponin, 2% bovine serum albumin, 1% fetal calf serum, and 1% donkey serum for 30 minutes, sections were labeled overnight at 4 °C with primary antibodies followed by washing in PBS before incubation for 1 hour at room temperature with secondary antibodies. Sections were then washed and blocked with sera of primary antibody species for 30 minutes, before staining in the same blocking buffer with fluorochrome-coupled antibodies for 1 hour. Slides were mounted in ProLong Gold ThermoFisher Scientific (Waltham, MA, USA) and observed with a Zeiss LSM 780 confocal microscope (Carl Zeiss, Oberkochen, Germany) using the spectral imaging mode[45]. Images were analyzed using Adobe Photoshop CC 2019 (Adobe systems, San Jose, CA).

To quantify cells expressing TCF7, we found that TCF7 was expressed by many helper T cells. Identification of $TCF7^+$ phagocytes was first performed by determining $SIRP\alpha^+$ phagocytes (cDC2s and LysoDCs) in $CD4^-TCF7^+$ cells (no helper T cells or LysoMacs). Then, within the $TCF7^+SIRP\alpha^+CD4^-$ cells, $CD101^+$ (DAV cDC2s) and $CX3CR1^+$ (LysoDCs) cells were identified. Other $TCF7^+SIRP\alpha^+$ phagocytes were assumed to be dome cDC2s.

The percentage of the area of CD101 and S100A4 staining was determined in an IFR of the last ileal PP for each mouse. The measurement was performed on 50,000 μm^2 IFR area (sections containing IFRs with area < 50,000 μm^2 were discarded) using a custom Fiji macro available from GitHub (https://github.com/Imagimm-CIML/Area-percentage-quantification).

Cell extraction

A minimum of three mice per experiment were used for extraction of PP phagocytes. PPs were digested with collagenase II/DNase I as previously described[31]. $CD11c^+$ cells were sorted using anti-CD11c microbeads and an AutoMACS magnetic cell separator according to manufacturer's instructions (Miltenyi Biotec, Bergisch Gladbach, Germany). The small intestines devoid of PPs were cut longitudinally in half and washed in a Petri dish with PBS. They were cut into 2 mm^2 pieces in complete medium containing 1mM Dithiothreitol (DTT) and were washed quickly in cold Hank's Balanced Salt Solution (HBSS) containing 2% FCS. Intestinal epithelial cells were removed by incubating tissues in Ethylenediaminetetraacetic acid (EDTA) buffer (HBSS, EDTA 2 mM) at 37 °C for 20 minutes in a shaker. This step was repeated once after a quick wash with HBSS buffer. Tissues were then digested with collagenase VIII (1 mg/ml) and DNAse I (200 µg/ml) at 37 °C in a shaker for 15 minutes. Digestion was stopped by adding 20 ml of cold PEF 2%. Debris were removed by filtration with a 70 µm cell strainer.

Flow cytometry and cell sorting

Cells were preincubated on ice for 5 minutes with 2.4G2 antibody to block Fc receptors and stained for surface markers. Cell mortality was evaluated using LIVE/DEAD™ Fixable Blue Dead Cell Stain Kit (ThermoFisher Scientific Waltham, MA, USA). Intracellular staining was performed using eBioscience™ Intracellular Fixation & Permeabilization Buffer Set according to manufacturer's instructions (ThermoFisher Scientific Waltham, MA, USA). Multiparametric flow cytometry and cell sorting were performed using a FACS LSRII UV and a FACSAria III (BD Biosciences, San Jose, CA, USA)), respectively. Data were analyzed with Flow Jo software (BD Biosciences, San Jose, CA, USA).

Statistical analysis

Results were compared with GraphPad Prism 8 software (GraphPad Software, La Jolla, CA, USA) using nonparametric Kruskal-Wallis with Dunn's multiple comparisons tests or Mann-Whitney t-test.

Single-cell RNA sequencing analysis

Libraries were prepared from mRNA of sorted cDC1s, cDC2s, LysoDCs, and LysoMacs extracted from Peyer's patches of 12 untreated, 12 R848-treated and 12 CpG-treated C57BL/6Rj female mice, using the Chromium Single-Cell 3′ kit from 10X Genomics (Pleasanton, CA, USA). Numbers of sorted cells to be sequenced were adjusted to allow good representativeness of all subsets as detailed in Supplementary Table 1. Next-generation sequencing was performed by UCAGenomiX (Institut de Pharmacologie Moleculaire et Cellulaire, Valbonne, France) using the NextSeq 500/550 High Output Kit v2 (75 cycles) cartridges from Illumina (San Diego, CA, USA) for the sequencing. FASTQ raw files were aligned to the mouse mm10 genome using Cell Ranger software version 2.0 (10X Genomics, Pleasanton, CA, USA), which performs filtering, barcode, and unique molecular identifier (UMI) counting. Quality control was performed to identify poor-quality cells for downstream analyses. Cells with less than 200 or more than 4000 (potential doublets) detected genes and cells with more than 10% mitochondrial gene expression (apoptotic cells) or less than 5% ribosomal genes were excluded from analyses. Dimensionality reduction and clustering were performed using UMAP embedding map colored by Seurat clustering. Clusters of cells were identified with Louvain algorithm provided by Seurat method 'FindClusters'. Marker genes for each cluster were extracted with Wilcoxon method using Seurat function 'FindMarkers' (Detailed parameters in technical reports). RNA velocity analysis was performed with scVelo[23].

Integration with intestinal cDC dataset

Guendel *et al.* raw data (fastq files)[24] of "wild-type" sample were downloaded from arrayexpress (E-MTAB-9522) and aligned to mouse genome (mm10 2020A) using CellRanger pipeline version 6.0.1 (10X Genomics, Pleasanton, CA, USA)) with an expected cell number of 8000. Resulting gene expression matrix was loaded in a Seurat object (min. 200 features by cell, and three cells by feature). Poor-quality cells were excluded from analysis as above to prevent enrichment of damaged cells or multiplets. Data were log-normalized (scale factor 10000) and centered, before detection of highly variable genes (top 2000). From a principal component analysis based on selected genes, the top 20 most informative dimensions were used for computing a two-dimensional non-linear projection of cells with UMAP algorithm. A Jaccard index was used to compare pairs of marker genes previously identified for each cluster of PP dataset to the markers detected for each cluster of Guendel *et al.* study[24] *w*ith Seurat 'FindMarkers' method (20 PCA dimensions, Wilcoxon, positive markers only, p value < 0.001).

AUTHOR CONTRIBUTIONS

Conceptualization, H.L.; Methodology, C.A.P., and H.L.; Investigation, C.A.P., R.F., C.W., C.L., M.L., C.D.S., F.H., J.T., and H.L.; Formal Analysis, R.F., L.S., M.F., C.A.P., and H.L.; Writing-Original Draft, H. L.; Writing-Review & Editing, C.A.P., H.L., and J.P.G.; Supervision, Project Administration and Funding Acquisition; H.L. and J.P.G.

DECLARATIONS OF COMPETING INTEREST

The authors declare no conflict of interests.

FUNDING

This work was supported by institutional funding from Centre National de la Recherche Scientifique and Institut National de la Santé et de la Recherche Médicale, by the Agence Nationale de la Recherche ANR-20-CE15-0016, and by Fondation pour la Recherche Médicale (FRM), grant number DEQ20170336745. F. H.V. was supported by the Infectiopôle Sud (Marseille) and the University of Honduras. C.D.S. and C.A.P. were supported by the FRM fellowship FDT20160434982 and the University of Costa Rica, respectively.

MATERIALS & CORRESPONDENCE

Correspondence and material requests should be addressed to Hugues Lelouard, lelouard@ciml.univ-mrs.fr.

ACKNOWLEDGMENTS

We thank Andreas Diefenbach and Frederik F. Heinrich for having helped us to re-analyze their single-cell RNA sequencing data on intestinal conventional dendritic cells. We acknowledge the PICSL imaging facility of the Centre d'Immunologie de Marseille-Luminy (CIML) (ImagImm), member of the national infrastructure France-BioImaging supported by the French National Research Agency (ANR-10-INBS-0004), the Computational Biology, Biostatistics and Modeling group (CB2M), the histology, the cytometry and the genomics core facilities of the CIML for expert assistance. We acknowledge Kevin Lebrigand, Virginie Magnone, and the UCAGenomiX platform, partner of the National Infrastructure France Génomique, supported by the Commissariat Aux Grands Investissements (ANR-10-INBS-0009) for sequencing our samples. We thank Pierre Milpied and Laurine Gil for helpful discussion and technical expertise in single-cell RNA sequencing.

APPENDIX A. SUPPLEMENTARY DATA

Supplementary data to this article can be found online at https://doi.org/10.1016/j.mucimm.2023.05.009.

References

1. Jung, C., Hugot, J. P. & Barreau, F. Peyer's patches: the immune sensors of the intestine. *Int. J. Inflam.* **2010**:823710.
2. Craig, S. W. & Cebra, J. J. Peyer's patches: an enriched source of precursors for IgA-producing immunocytes in the rabbit. *J. Exp. Med.* **134**, 188–200 (1971).
3. Reboldi, A. & Cyster, J. G. Peyer's patches: organizing B-cell responses at the intestinal frontier. *Immunol. Rev.* **271**, 230–245 (2016).
4. Da Silva, C., Wagner, C., Bonnardel, J., Gorvel, J. P. & Lelouard, H. The Peyer's patch mononuclear phagocyte system at steady state and during infection. *Front. Immunol.* **8**, 1254 (2017).
5. Lelouard, H. et al. Pathogenic bacteria and dead cells are internalized by a unique subset of Peyer's patch dendritic cells that express lysozyme. *Gastroenterology* **138**, 173–184.e1 (2010).
6. Bonnardel, J. et al. Innate and adaptive immune functions of Peyer's patch monocyte-derived cells. *Cell Rep.* **11**, 770–784 (2015).
7. Wagner, C. et al. Differentiation paths of Peyer's patch LysoDCs are linked to sampling site positioning, migration, and T cell priming. *Cell Rep.* **31**:107479.
8. Lelouard, H., Fallet, M., de Bovis, B., Méresse, S. & Gorvel, J. P. Peyer's patch dendritic cells sample antigens by extending dendrites through M cell-specific transcellular pores. *Gastroenterology* **142**, 592–601.e3 (2012).
9. Martínez-López, M. et al. Microbiota sensing by Mincle-Syk axis in dendritic cells regulates interleukin-17 and -22 production and promotes intestinal barrier integrity. *Immunity* **50**, 446–461.e9 (2019).
10. Kim, S. H., Cho, B. H., Kim, K. S. & Jang, Y. S. Complement C5a promotes antigen cross-presentation by Peyer's patch monocyte-derived dendritic cells and drives a protective CD8+ T cell response. *Cell Rep.* **35**:108995.
11. Becker, M. et al. Ontogenic, phenotypic, and functional characterization of XCR1(+) dendritic cells leads to a consistent classification of intestinal dendritic cells based on the expression of XCR1 and SIRPalpha. *Front. Immunol.* **5**, 326 (2014).
12. Iwasaki, A. & Kelsall, B. L. Localization of distinct Peyer's patch dendritic cell subsets and their recruitment by chemokines macrophage inflammatory protein (MIP)-3alpha, MIP-3beta, and secondary lymphoid organ chemokine. *J. Exp. Med.* **191**, 1381–1394 (2000).
13. Bonnardel, J. et al. Distribution, location, and transcriptional profile of Peyer's patch conventional DC subsets at steady state and under TLR7 ligand stimulation. *Mucosal Immunol.* **10**, 1412–1430 (2017).
14. Wagner, C. et al. Some news from the Unknown Soldier, the Peyer's patch macrophage. *Cell. Immunol.* **330**, 159–167 (2018).
15. Hanawa-Suetsugu, K. et al. Phagocytosis is mediated by two-dimensional assemblies of the F-BAR protein GAS7. *Nat. Commun.* **10**, 4763 (2019).
16. Jinnohara, T. et al. IL-22BP dictates characteristics of Peyer's patch follicle-associated epithelium for antigen uptake. *J. Exp. Med.* **214**, 1607–1618 (2017).
17. Miller, J. C. et al. Deciphering the transcriptional network of the dendritic cell lineage. *Nat. Immunol.* **13**, 888–899 (2012).
18. Bosteels, C. et al. Inflammatory Type 2 cDCs acquire features of cDC1s and macrophages to orchestrate immunity to respiratory virus infection. *Immunity* **52**, 1039–1056.e9 (2020).
19. Scott, C. L. et al. CCR2(+)CD103(-) intestinal dendritic cells develop from DC-committed precursors and induce interleukin-17 production by T cells. *Mucosal Immunol.* **8**, 327–339 (2015).
20. Kunimura, K. et al. S100A4 protein is essential for the development of mature microfold cells in Peyer's patches. *Cell Rep.* **29**, 2823–2834.e7 (2019).
21. Wu, X. et al. Bcl11a controls Flt3 expression in early hematopoietic progenitors and is required for pDC development in vivo. *PLoS One* **8**, e64800 (2013).
22. Schlitzer, A. et al. Identification of cDC1- and cDC2-committed DC progenitors reveals early lineage priming at the common DC progenitor stage in the bone marrow. *Nat. Immunol.* **16**, 718–728 (2015).
23. Bergen, V., Lange, M., Peidli, S., Wolf, F. A. & Theis, F. J. Generalizing RNA velocity to transient cell states through dynamical modeling. *Nat. Biotechnol.* **38**, 1408–1414 (2020).
24. Guendel, F. et al. Group 3 innate lymphoid cells program a distinct subset of IL-22BP-Producing dendritic cells demarcating solitary intestinal lymphoid tissues. *Immunity* **53**, 1015–1032.e8 (2020).
25. Wang, Y. et al. Inhibitory/suppressive oligodeoxynucleotide nanocapsules as simple oral delivery devices for preventing atopic dermatitis in mice. *Mol. Ther.* **23**, 297–309 (2015).
26. Mora, J. R. et al. Selective imprinting of gut-homing T cells by Peyer's patch dendritic cells. *Nature* **424**, 88–93 (2003).

27. Mora, J. R. et al. Generation of gut-homing IgA-secreting B cells by intestinal dendritic cells. *Science* **314**, 1157–1160 (2006).
28. Reboldi, A. et al. IgA production requires B cell interaction with subepithelial dendritic cells in Peyer's patches. *Science* **352**, aaf4822 (2016).
29. Luciani, C., Hager, F. T., Cerovic, V. & Lelouard, H. Dendritic cell functions in the inductive and effector sites of intestinal immunity. *Mucosal Immunol.* **15**, 40–50 (2022).
30. Tamoutounour, S. et al. CD64 distinguishes macrophages from dendritic cells in the gut and reveals the Th1-inducing role of mesenteric lymph node macrophages during colitis. *Eur. J. Immunol.* **42**, 3150–3166 (2012).
31. Bonnardel, J. H. et al. Gene expression profiling of the Peyer's patch mononuclear phagocyte system. *Genom. Data* **5**, 21–24 (2015).
32. Durai, V. et al. Altered compensatory cytokine signaling underlies the discrepancy between Flt3(-/-) and Flt3l(-/-) mice. *J. Exp. Med.* **215**, 1417–1435 (2018).
33. Waskow, C. et al. The receptor tyrosine kinase Flt3 is required for dendritic cell development in peripheral lymphoid tissues. *Nat. Immunol.* **9**, 676–683 (2008).
34. Kawaguchi, M. et al. Hepatocyte growth factor activator inhibitor-2 stabilizes Epcam and maintains epithelial organization in the mouse intestine. *Commun. Biol.* **2**, 11 (2019).
35. Szabo, R., Callies, L. K. & Bugge, T. H. Matriptase drives early-onset intestinal failure in a mouse model of congenital tufting enteropathy. *Development* **146**, dev183392 (2019).
36. Kimura, S. et al. Visualization of the entire differentiation process of murine M cells: suppression of their maturation in cecal patches. *Mucosal Immunol.* **8**, 650–660 (2015).
37. Park, K. et al. The transcription factor NR4A3 controls CD103+ dendritic cell migration. *J. Clin. Invest.* **126**, 4603–4615 (2016).
38. Pasare, C. & Medzhitov, R. Control of B-cell responses by toll-like receptors. *Nature* **438**, 364–368 (2005).
39. Wallace, C. H. et al. B lymphocytes confer immune tolerance via cell surface GARP-TGF-β complex. *JCI Insight* **3**, e99863 (2018).
40. Cong, Y., Feng, T., Fujihashi, K., Schoeb, T. R. & Elson, C. O. A dominant, coordinated T regulatory cell-IgA response to the intestinal microbiota. *PNAS* **106**, 19256–19261 (2009).
41. Gribonika, I. et al. Class-switch recombination to IgA in the Peyer's patches requires natural thymus-derived Tregs and appears to be antigen independent. *Mucosal Immunol.* **12**, 1268–1279 (2019).
42. Tsuji, M. et al. Preferential generation of follicular B helper T cells from Foxp3+ T cells in gut Peyer's patches. *Science* **323**, 1488–1492 (2009).
43. Faust, N., Varas, F., Kelly, L. M., Heck, S. & Graf, T. Insertion of enhanced green fluorescent protein into the lysozyme gene creates mice with green fluorescent granulocytes and macrophages. *Blood* **96**, 719–726 (2000).
44. Jung, S. et al. Analysis of fractalkine receptor CX(3)CR1 function by targeted deletion and green fluorescent protein reporter gene insertion. *Mol. Cell Biol.* **20**, 4106–4114 (2000).
45. Lelouard, H., Mailfert, S. & Fallet, M. A ten-color spectral imaging strategy to reveal localization of gut immune cell subsets. *Zeiss Application note* 2018. https://doi.org/10.13140/RG.2.2.18840.88324. https://www.zeiss.fr/content/dam/Microscopy/fr/download/note_application_a_ten_color.pdf.